Contents

10 Cosmic microwave background **177**
10.1 Introducing the CMB anisotropies . . . 177
10.2 Multipole analysis . . . 181
10.2.1 Spherical harmonics . . . 182
10.2.2 The theoretical angular power spectrum . . . 184
10.2.3 Observed angular power spectrum . . . 185
10.2.4 Cosmic variance . . . 185
10.3 Multipoles and scales . . . 186
10.3.1 Rough correspondence . . . 186
10.3.2 Exact treatment . . . 187
10.4 Important distance scales on the last scattering surface . . . 191
10.4.1 Angular diameter distance to the last scattering surface . . . 191
10.4.2 Decoupling scale and the matter-radiation equality scale . . . 193
10.5 CMB anisotropy from perturbation theory . . . 195
10.6 Large scales: Sachs–Wolfe part of the spectrum . . . 197
10.6.1 Angular power spectrum from the ordinary Sachs–Wolfe effect 197
10.7 Acoustic oscillations . . . 199
10.8 Diffusion damping . . . 204
10.9 The complete C_ℓ spectrum . . . 207
10.10 Cosmological parameters and CMB anisotropy . . . 207
10.10.1 Independent vs. dependent parameters . . . 211
10.10.2 Sound horizon angle . . . 212
10.10.3 Acoustic peak heights . . . 215
10.10.4 Effect of Ω_0 and $\Omega_{\Lambda 0}$ . . . 216
10.10.5 Effect of the primordial spectrum . . . 220
10.10.6 Effect of the optical depth due to reionisation . . . 220
10.10.7 Effect of ω_b and ω_m . . . 220
10.11 Values of the cosmological parameters . . . 225

10 Cosmic microwave background

10.1 Introducing the CMB anisotropies

The CMB is very isotropic. Assuming we are not in a special position in the universe, this tells us that the early universe was very homogeneous and isotropic at $t = t_{\text{dec}} \approx$ 380 000 years, when the CMB was formed. The small anisotropy of the CMB reflects the small perturbations in the early universe.

This anisotropy was first detected in 1992 by the DMR instrument on the COBE satellite, which mapped the whole sky on three microwave frequencies. The angular resolution of COBE was 7°, so it could only detect features larger than this, and there is much more information on smaller scales. The 2006 Nobel prize in physics was awarded to John C. Mather and George F. Smoot for showing that the CMB spectrum has a blackbody shape and for measuring the anisotropy. Measurements with better resolution, but covering only small parts of the sky, were then performed with instruments carried by balloons to the upper atmosphere and ground-based detectors located at high altitudes.

The second full-sky map of the CMB was made by the Wilkinson Microwave Anisotropy Probe (WMAP) satellite, in orbit around the L2 point of the Sun-Earth system, 1.5 million kilometers from the Earth in the direction opposite to the Sun. The NASA satellite was launched in 2001, and the results of the first year of measurements were published in 2003. The WMAP satellite made eight years of measurements, and the the final data release was in 2012. The third and so far the most precise full-sky measurement was made by ESA's Planck satellite, which was launched in 2009. The first cosmological results were released in 2013, and the final data release was in 2018.

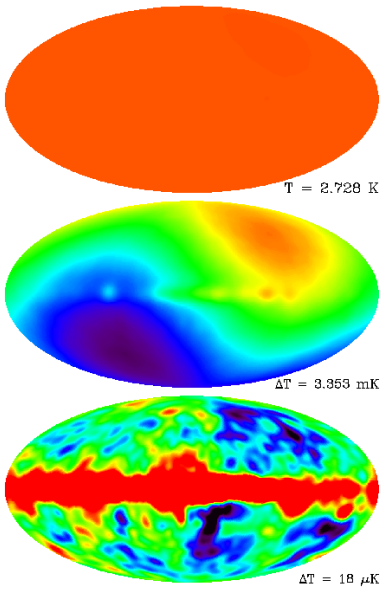


Figure 1: The cosmic microwave sky as seen by the DMR instrument aboard the COBE satellite. The top image shows the radiation without removing the monopole, the second without removing the dipole, and the third without removing foreground contamination. (Source: https://lambda.gsfc.nasa.gov/product/cobe/dmr_image.html.)

Figure 1 shows the microwave sky measured by COBE satellite, with successive removal of the monopole and dipole component, and figure 2 shows the microwave sky after subtracting the monopole, dipole and foreground sources in the Milky Way and outside: what remains is the $\left(\frac{\delta T}{T}\right)_{\text{obs}}$ of the CMB. Figures 3 and 4 show final measurements of the WMAP and Planck satellites, respectively. Red and yellow mean hotter than average, blue means colder than average.

The CMB photons have have travelled to us from the intersection of our past light cone and the hypersurface where photons decouple at $t = t_{\text{dec}}$. This intersection forms a sphere called the *last scattering surface*[1]. We are at the center of this sphere, which extends away from us both in space and in time.

[1]Or the *last scattering sphere*. The expression "last scattering surface" is sometimes also used to refer to the entire $t = t_{\text{dec}}$ time slice.

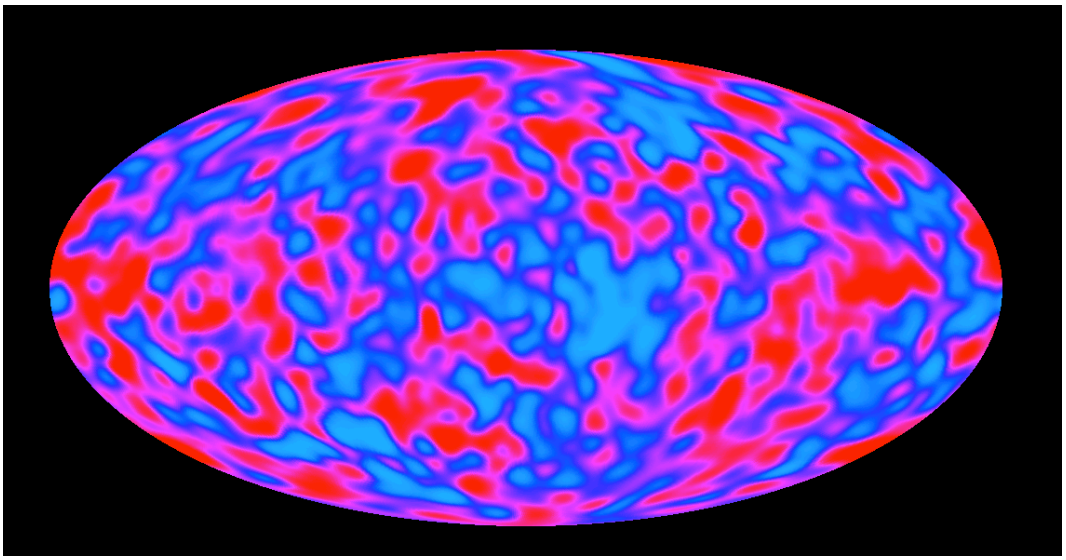


Figure 2: The CMB according to the DMR instrument aboard the COBE satellite. (Source: https://lambda.gsfc.nasa.gov/product/cobe/dmr_image.html.)

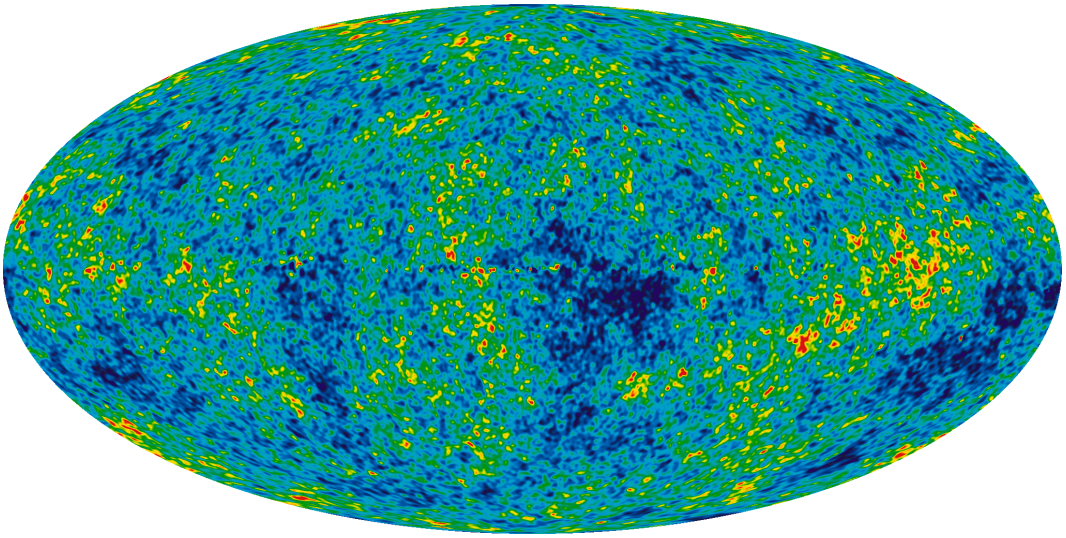


Figure 3: The CMB according to the WMAP satellite. (Source: https://map.gsfc.nasa.gov/media/101080/index.html.)

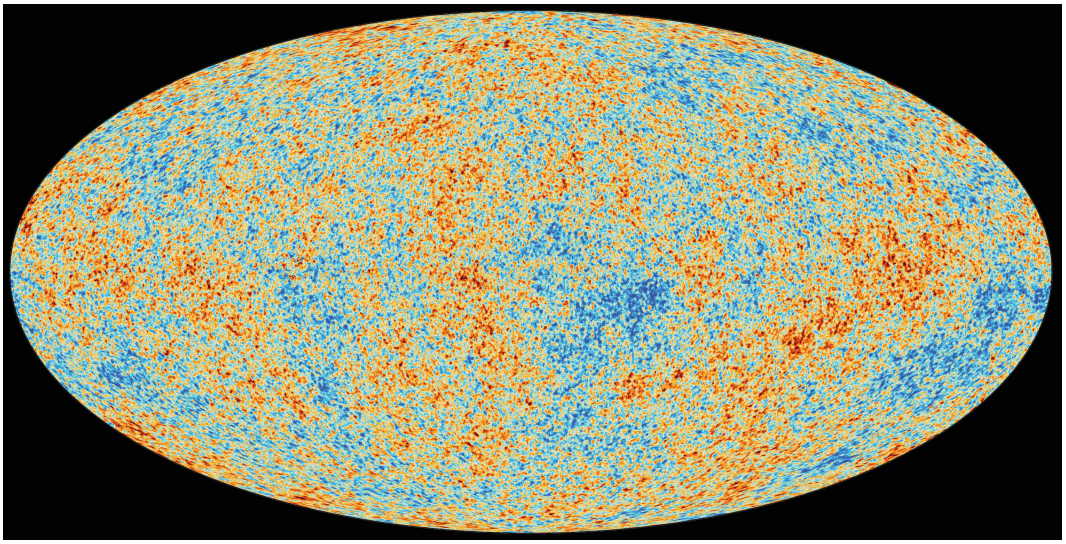


Figure 4: The CMB according to the Planck satellite. (Source: https://www.esa.int/ESA_Multimedia/Images/2018/07/Planck_s_view_of_the_cosmic_microwave_background.)

The observed temperature anisotropy can be split into two contributions, an intrinsic temperature variation at the surface of last scattering and a variation in the redshift the photons during their journey,

$$\left(\frac{\delta T}{T}\right)_{\text{obs}} = \left(\frac{\delta T}{T}\right)_{\text{intr}} + \left(\frac{\delta T}{T}\right)_{\text{jour}} . \tag{10.1}$$

See figure 5. This split is convenient but coordinate-dependent, only the sum is an observable quantity. There are two physically different ways to define what we mean by the CMB perturbation δT. The first is to take the average of the temperature field over the sky and call this the mean, $\bar{T} \equiv T_0 \equiv \frac{1}{4\pi}\int d\Omega T$, and define the anisotropy as the deviation from the mean, $\delta T = T - T_0$. However, in the context of perturbed FLRW models, it can be simpler to denote the deviation of the temperature from that of the background model by δT instead. As the perturbation also contributes to the mean temperature, this second definition is not equivalent to the first one. However, as the contribution to the perturbations to the mean is very small compared to the background contribution, the difference is usually negligible. As is customary, we will use the notation $\frac{\delta T}{T}$ instead of $\frac{\delta T}{\bar{T}}$ or $\frac{\delta T}{T_0}$, but it should be understood that the temperature in the denominator is the mean temperature. (This would only make a difference at second order and higher orders in the perturbations, and we only consider linear perturbation theory.)

The first term in (10.1), $\left(\frac{\delta T}{T}\right)_{\text{intr}}$ represents the temperature variation of the photon gas at $t = t_{\text{dec}}$. (It also includes the Doppler effect from the motion of

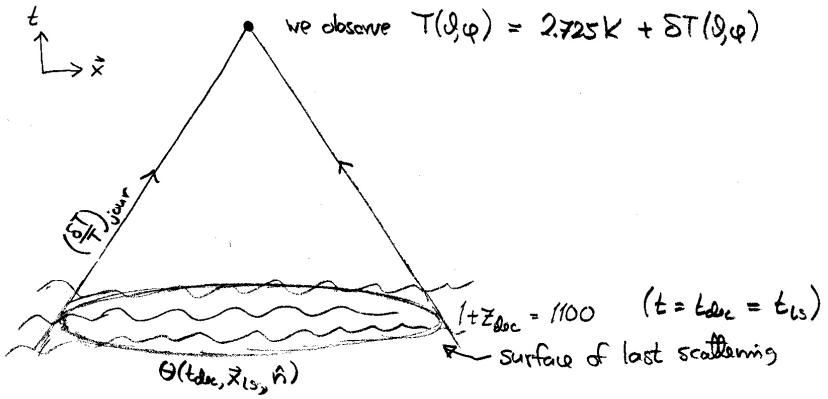


Figure 5: The observed CMB temperature anisotropy gets a contribution from the last scattering surface, $(\delta T/T)_{\rm intr} = \Theta(t_{\rm dec}, \boldsymbol{x}_{\rm ls}, \hat{\boldsymbol{n}})$ and from along the photon's journey to us, $(\delta T/T)_{\rm jour}$.

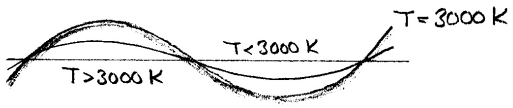


Figure 6: Depending on the gauge, the $T_{\rm dec}$ = constant surface may or may not (and usually does not) coincide with the $t = t_{\rm dec}$ time slice.

this photon gas.) At that time the largest scales we see on the CMB sky were still outside the Hubble radius. The separation of $\delta T/T$ into two components is gauge-dependent. If the time slice $t = t_{\rm dec}$ dips further into the past in some location, it finds a higher temperature, but the photons from there also have then a longer way to go and suffer a larger redshift, so the two effects balance each other. We can calculate in any gauge we want, getting different results for $(\delta T/T)_{\rm intr}$ and $(\delta T/T)_{\rm jour}$ depending on the gauge, but their sum $(\delta T/T)_{\rm obs}$ is gauge-independent, because it is an observed quantity.

One might think that $(\delta T/T)_{\rm intr}$ should be equal to zero, since in our earlier discussion of recombination and decoupling we identified decoupling with a particular temperature $T_{\rm dec} \sim 3000$ K. This kind of thinking corresponds to a particular gauge choice where the $t = t_{\rm dec}$ time slice coincides with the $T = T_{\rm dec}$ hypersurface. In this gauge $(\delta T/T)_{\rm intr} = 0$, except for the Doppler effect (we are not going to use this gauge). Anyway, it is not true that all photons have their last scattering exactly when $T = T_{\rm dec}$. Rather they occur during a rather large temperature interval and time period. The zeroth-order (background) time evolution of the temperature of the photon distribution is the same before and after last scattering, $T \propto a^{-1}$, so it does not matter how we draw the artificial separation line, the time slice $t = t_{\rm dec}$ separating the fluid and free particle treatment of the photons. See figure 6.

10.2 Multipole analysis

The CMB temperature anisotropy is a function on a sphere. In analogy with Fourier expansion in three-dimensional flat space, we separate out the contributions of dif-

ferent angular scales with a multipole expansion,

$$\frac{\delta T}{T_0}(\theta,\phi) = \sum a_{\ell m} Y_{\ell m}(\theta,\phi) \ , \tag{10.2}$$

where the sum runs over $l = 1, 2, \ldots, \infty$ and $m = -\ell, \ldots, \ell$, giving $2\ell + 1$ values of m for each ℓ. The functions $Y_{\ell m}(\theta,\phi)$ are the *spherical harmonics*, which form an orthonormal set of functions over the sphere (see figure 7). Another notation for $Y_{\ell m}(\theta,\phi)$ is $Y_{\ell m}(\hat{\boldsymbol{n}})$, where $\hat{\boldsymbol{n}}$ is a unit vector whose direction is specified by the angles θ and ϕ. (The hat denotes unit vector.) Using the orthonormality, we can calculate the multipole coefficients $a_{\ell m}$ as

$$a_{\ell m} = \int Y^*_{\ell m}(\theta,\phi) \frac{\delta T}{T_0}(\theta,\phi) \mathrm{d}\Omega \ . \tag{10.3}$$

This definition gives dimensionless $a_{\ell m}$. Often $a_{\ell m}$ are instead defined without dividing by $T_0 = 2.725$ K, in which case they have the dimension of temperature and are usually given in units of μK.

The coefficient $a_{\ell 0}$ is real but the other $a_{\ell m}$ are complex, and $a_{\ell,-m} = a^*_{\ell m}$. The sum begins at $\ell = 1$, since $Y_{00} =$ constant, so we have $a_{00} = 0$ for a quantity that represents deviation from average. The dipole part, $\ell = 1$, is dominated by the Doppler effect due to the motion of the solar system with respect to the last scattering surface, and it is difficult to separate the *cosmological dipole* caused by large scale perturbations. This was done for the first time with Planck, though not to great accuracy. If we assume that the vast majority of the dipole is due to our motion, the velocity of the Solar system with respect to the CMB is $v = 369$ km/s $= 1.23 \times 10^{-3}$. Without this assumption we get $v = 384 \pm 139$ km/s [1]. Our motion with respect to the CMB also generates higher multipoles, but these contributions are suppressed as v^ℓ. So the amplitude of this kinetic contribution to the quadrupole ($\ell = 3$) is $\sim 10^{-6}$, and higher powers are negligible. We consider only the $\ell \geq 2$ part of the expansion, and neglect the contributions due to our motion to the higher multipoles.

10.2.1 Spherical harmonics

We list here some useful properties of the spherical harmonics. They are orthonormal functions on the sphere, so

$$\int \mathrm{d}\Omega \ Y_{\ell m}(\theta,\phi) Y^*_{\ell' m'}(\theta,\phi) = \delta_{\ell\ell'}\delta_{mm'} \ . \tag{10.4}$$

Summing over the m corresponding to the same multipole number ℓ, we have the *closure relation*

$$\sum_m |Y_{\ell m}(\theta,\phi)|^2 = \frac{2\ell+1}{4\pi} \ . \tag{10.5}$$

We will also have use for the expansion of a plane wave in terms of spherical harmonics,

$$e^{i\boldsymbol{k}\cdot\boldsymbol{x}} = 4\pi \sum_{\ell m} i^\ell j_\ell(kx) Y_{\ell m}(\hat{\boldsymbol{x}}) Y^*_{\ell m}(\hat{\boldsymbol{k}}) \ . \tag{10.6}$$

Here $\hat{\boldsymbol{x}}$ and $\hat{\boldsymbol{k}}$ are the unit vectors in the directions of $\boldsymbol{x}$ and $\boldsymbol{k}$, and j_ℓ is the spherical Bessel function.

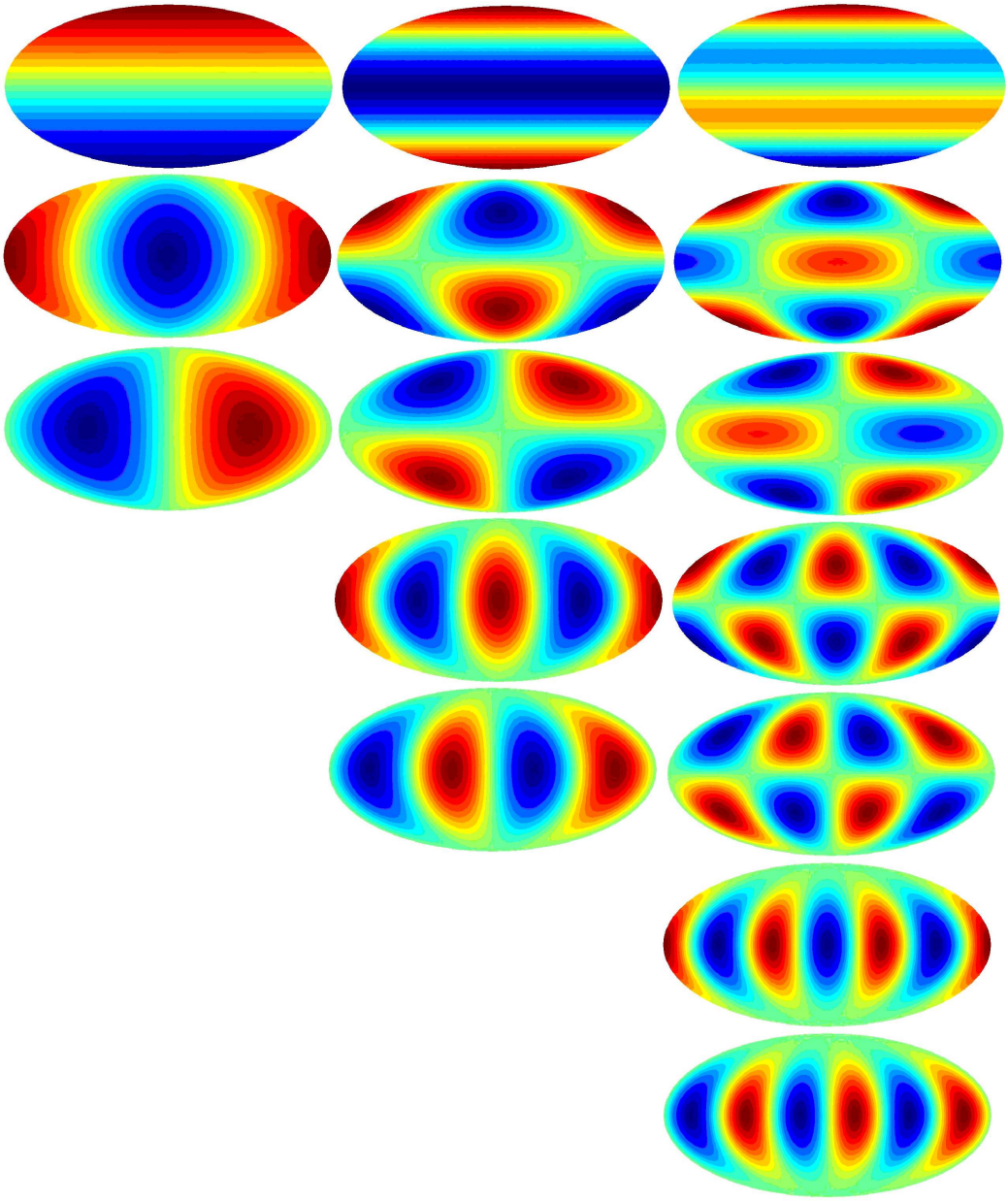


Figure 7: The three lowest multipoles $\ell = 1, 2, 3$ of spherical harmonics. Left column: Y_{10}, Re , Y_{11}, Im , Y_{11}. Middle column: Y_{20}, Re , Y_{21}, Im , Y_{21}, Re , Y_{22}, Im , Y_{22}. Right column: Y_{30}, Re , Y_{31}, Im , Y_{31}, Re , Y_{32}, Im , Y_{32}, Re , Y_{33}, Im , Y_{33}. Figure by Ville Heikkilä.

10.2.2 The theoretical angular power spectrum

The part of the CMB anisotropy that is not due to our motion is due to the primordial perturbations, and therefore reflects their Gaussian nature. Because we get the values of the $a_{\ell m}$ from the other perturbation quantities through linear equations (in first order perturbation theory), the $a_{\ell m}$ are also (complex) Gaussian random variables. Since they represent deviation from the average temperature, their expectation value is zero,

$$\langle a_{\ell m} \rangle = 0 \ , \tag{10.7}$$

and the quantity we want to calculate from theory is the variance $\langle |a_{\ell m}|^2 \rangle$ to get a prediction for the typical amplitude of $a_{\ell m}$. The isotropic nature of the random process means that these expectation values depend only on ℓ, not m. (The ℓ are related to the angular size of the anisotropy pattern, whereas the m are related to its orientation.) Since $\langle |a_{\ell m}|^2 \rangle$ is independent of m, we can define

$$C_\ell \equiv \langle |a_{\ell m}|^2 \rangle = \frac{1}{2\ell+1} \sum_m \langle |a_{\ell m}|^2 \rangle \ . \tag{10.8}$$

The quantities $a_{\ell m}$ are independent random variables, so

$$\langle a_{\ell m} a^*_{\ell' m'} \rangle = \delta_{\ell\ell'} \delta_{mm'} C_\ell \ . \tag{10.9}$$

This function C_ℓ (of integers $\ell \geq 1$) is called the (theoretical) *angular power spectrum*. It is analogous to the power spectrum $\mathcal{P}(k)$ of density perturbations. For Gaussian perturbations, C_ℓ contains all the statistical information about the CMB temperature anisotropy. This is all we can predict from theory. Thus analysis of the CMB anisotropy consists of calculating the angular power spectrum from the observed CMB and comparing it to the C_ℓ predicted by theory.[2]

Just like the three-dimensional density power spectrum $\mathcal{P}(k)$ gives the contribution of scale k to the density variance $\langle \delta(\boldsymbol{x})^2 \rangle$, the angular power spectrum C_ℓ is related to the contribution of multipole ℓ to the temperature variance,

$$\begin{aligned} \left\langle \left(\frac{\delta T(\theta,\phi)}{T} \right)^2 \right\rangle &= \left\langle \sum_{\ell m} a_{\ell m} Y_{\ell m}(\theta,\phi) \sum_{\ell' m'} a^*_{\ell' m'} Y^*_{\ell' m'}(\theta,\phi) \right\rangle \\ &= \sum_{\ell\ell'} \sum_{mm'} Y_{\ell m}(\theta,\phi) Y^*_{\ell' m'}(\theta,\phi) \langle a_{\ell m} a^*_{\ell' m'} \rangle \\ &= \sum_\ell C_\ell \sum_m |Y_{\ell m}(\theta,\phi)|^2 = \sum_\ell \frac{2\ell+1}{4\pi} C_\ell \ , \end{aligned} \tag{10.10}$$

where we have used the closure relation (10.5) and the orthogonality relation (10.9).

Thus, if we plot $(2\ell+1)C_\ell/(4\pi)$ on a linear ℓ scale, or $\ell(2\ell+1)C_\ell/(4\pi)$ on a logarithmic ℓ scale, the area under the curve gives the temperature variance, i.e. the

[2] In addition to the temperature anisotropy, the CMB also has another property, its polarisation. There are two additional power spectra related to the polarisation, C_ℓ^{EE} and C_ℓ^{BB}, and one related to the correlation between temperature and polarisation, C_ℓ^{TE}. All of them have been measured, and contain interesting cosmological information, though the polarisation results are yet not as advanced as those of the temperature. The polarisation signal is weaker, so measuring it and distinguishing it from foreground contamination is more difficult.

expectation value for the squared deviation from the average temperature. It has become customary to plot the angular power spectrum as $\ell(\ell+1)C_\ell/(2\pi)$, which is neither of these, but for large ℓ approximates the second case. (The reason for this custom will become clear later.)

Equation (10.10) represents the expectation value from theory and thus it is the same for all directions $(\theta,\,\phi)$. The actual realised value of course varies from one direction to another. We can imagine an ensemble of universes, each representing a different realisation of the same random process that produces the primordial perturbations. The quantity $\langle\ \rangle$ represents the average over such an ensemble. (Note that we have again equated a quantum mechanical expectation value, predicted by inflation, with the expectation value over the realisations of a classical ensemble. This step has been the subject of much study, but is still not completely understood.)

10.2.3 Observed angular power spectrum

Theory predicts the expectation values $\langle|a_{\ell m}|^2\rangle$ from the random process responsible for the CMB anisotropy, but we can observe only one realisation of this random process, the set $\{a_{\ell m}\}$ of our CMB sky. We define the *observed* angular power spectrum as the average

$$\widehat{C}_\ell \equiv \frac{1}{2\ell+1}\sum_m |a_{\ell m}|^2 \tag{10.11}$$

of these observed values.

The variance of the observed temperature anisotropy is the average of $\left[\frac{\delta T(\theta,\phi)}{T}\right]^2$ over the celestial sphere,

$$\begin{aligned}
\frac{1}{4\pi}\int \mathrm{d}\Omega \left[\frac{\delta T(\theta,\phi)}{T}\right]^2 &= \frac{1}{4\pi}\int d\Omega \sum_{\ell m} a_{\ell m} Y_{\ell m}(\theta,\phi) \sum_{\ell' m'} a^*_{\ell' m'} Y^*_{\ell' m'}(\theta,\phi) \\
&= \frac{1}{4\pi}\sum_{\ell m}\sum_{\ell' m'} a_{\ell m} a^*_{\ell' m'} \underbrace{\int \mathrm{d}\Omega Y_{\ell m}(\theta,\phi) Y^*_{\ell' m'}(\theta,\phi)}_{\delta_{\ell\ell'}\delta_{mm'}} \\
&= \frac{1}{4\pi}\sum_{\ell} \underbrace{\sum_m |a_{\ell m}|^2}_{(2\ell+1)\widehat{C}_\ell} \\
&= \sum_\ell \frac{2\ell+1}{4\pi}\widehat{C}_\ell\ .
\end{aligned} \tag{10.12}$$

Equation (10.12) gives the variance of $\delta T/T$ of our given sky over the celestial sphere. Contrast this with (10.10), which gives the variance of $\delta T/T$ at an arbitrary location on the sky over different realisations of the random process that produced the primordial perturbations.

10.2.4 Cosmic variance

The expectation value of the observed spectrum $\widehat{C}_\ell$ is equal to C_ℓ, the *theoretical* spectrum (10.8), i.e.

$$\langle\widehat{C}_\ell\rangle = C_\ell \quad\Rightarrow\quad \langle\widehat{C}_\ell - C_\ell\rangle = 0\ , \tag{10.13}$$

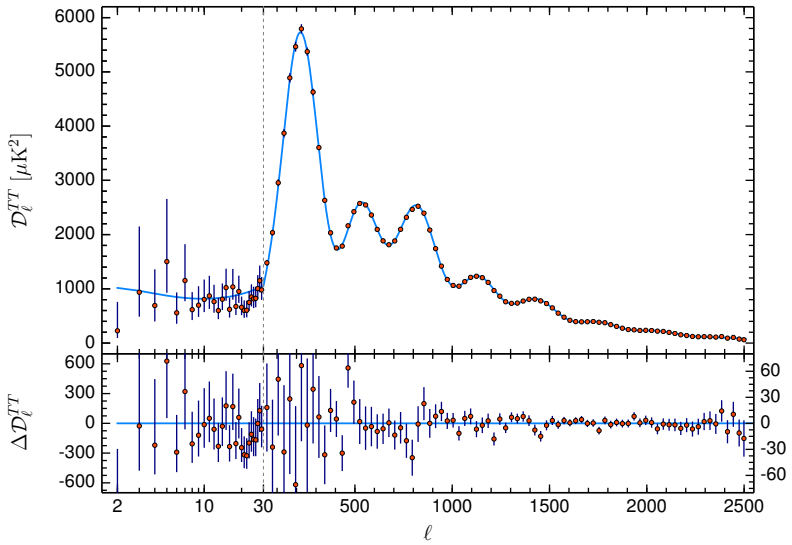


Figure 8: The observed angular power spectrum $\ell(\ell+1)\widehat{C}_\ell/(2\pi)$ according to the Planck satellite, in units of μK. The data points are measured values, and the error bars combine cosmic variance and instrumental errors: the former dominates except at very large ℓ. The solid curve is the theoretical curve from the best-fit ΛCDM model. The lower plot shows the difference between observations and the model fit.

but its actual, realised, value is not. The expected squared difference between $\widehat{C}_\ell$ and C_ℓ is called the *cosmic variance*. We can calculate it using the properties of (complex) Gaussian random variables (**Exercise.** Do this). The answer is

$$\langle(\widehat{C}_\ell - C_\ell)^2\rangle = \frac{2}{2\ell+1}C_\ell^2 \ . \tag{10.14}$$

The expected relative difference between $\widehat{C}_\ell$ and C_ℓ is smaller for higher ℓ. This is because we have a larger (size 2ℓ+1) statistical sample of $a_{\ell m}$ available for calculating the $\widehat{C}_\ell$. Cosmic variance limits the accuracy of comparison of CMB observations with theory, especially for large scales (small ℓ).

10.3 Multipoles and scales

10.3.1 Rough correspondence

The different multipole numbers ℓ correspond to different angular scales: low ℓ to large scales and high ℓ to small scales. The functions $Y_{\ell m}(\theta,\phi)$ have an oscillatory pattern on the sphere, and there are typically ℓ wavelengths of oscillation around a full great circle on the sphere. See figure 9. The angle corresponding to this wavelength is

$$\theta_\lambda = \frac{2\pi}{\ell} = \frac{360^\circ}{\ell} \ . \tag{10.15}$$

See figure 10. The angle corresponding to a half-wavelength, i.e. separation between a neighbouring minimum and maximum, is then

$$\theta_{\rm res} = \frac{\pi}{\ell} = \frac{180^\circ}{\ell} \ . \tag{10.16}$$

This is the angular resolution of the microwave detector required to resolve the angular power spectrum up to ℓ.

For example, COBE had an angular resolution of 7° allowing a measurement up to $\ell = 180/7 = 26$, WMAP had resolution 0.23° reaching to $\ell = 180/0.23 = 783$, and Planck had resolution $5'$ corresponding to $\ell = 2160$.[3] (In reality, there is no sharp cut-off at a particular ℓ, the error bars just grow rapidly.) Comparison with figure 8 shows that this rough approximation is correct only to an order of magnitude: the Planck error bars remain small to about $\ell = 2500$.

The angles on the sky are related to physical or comoving distances via the angular diameter distance d_A, defined as the ratio of the physical length (transverse to the line of sight) and the angle it covers, as discussed in chapter 3,

$$d_A = \frac{\lambda_{\rm phys}}{\theta} \ . \tag{10.17}$$

Likewise the comoving angular diameter distance d_A^c is

$$d_A^c = \frac{\lambda^c}{\theta} \ , \tag{10.18}$$

where $\lambda^c = (1/a)\lambda_{\rm phys} = (1+z)\lambda_{\rm phys}$ is the corresponding comoving length. Thus $d_A^c = (1/a)d_A = (1+z)d_A$. See figure 11.

Consider now the Fourier modes of our earlier perturbation theory discussion. A mode with comoving wavenumber k has comoving wavelength $\lambda^c = 2\pi/k$. Thus this mode should show up as a pattern on the CMB sky with angular size

$$\theta_\lambda = \frac{\lambda^c}{d_A^c} = \frac{2\pi}{k d_A^c} = \frac{2\pi}{\ell} \ . \tag{10.19}$$

For the last equality we used the relation (10.15). We see that modes with wavenumber k contribute mostly to multipoles around

$$\ell = k d_A^c \ . \tag{10.20}$$

10.3.2 Exact treatment

The above matching of wavenumbers with multipoles is rather naive, for two reasons:

1. The description of a spherical harmonic $Y_{\ell m}$ having an "angular wavelength" of $2\pi/\ell$ is just a crude characterisation. See figure 9.

2. The modes $\boldsymbol{k}$ are not wrapped around the sphere of last scattering, but the wave vector forms a different angle with the sphere at different places.

The following precise discussion applies only for the case of a spatially flat background, where on a slice of constant time we can Fourier expand functions. Consider some function

$$f(\boldsymbol{x}) = \sum_{\boldsymbol{k}} f_{\boldsymbol{k}} e^{i\boldsymbol{k}\cdot\boldsymbol{x}} \tag{10.21}$$

[3] One angle ($^\circ$) is divided into 60 arcminutes ($'$) and each arcminute is divided into 60 arcseconds ($''$).

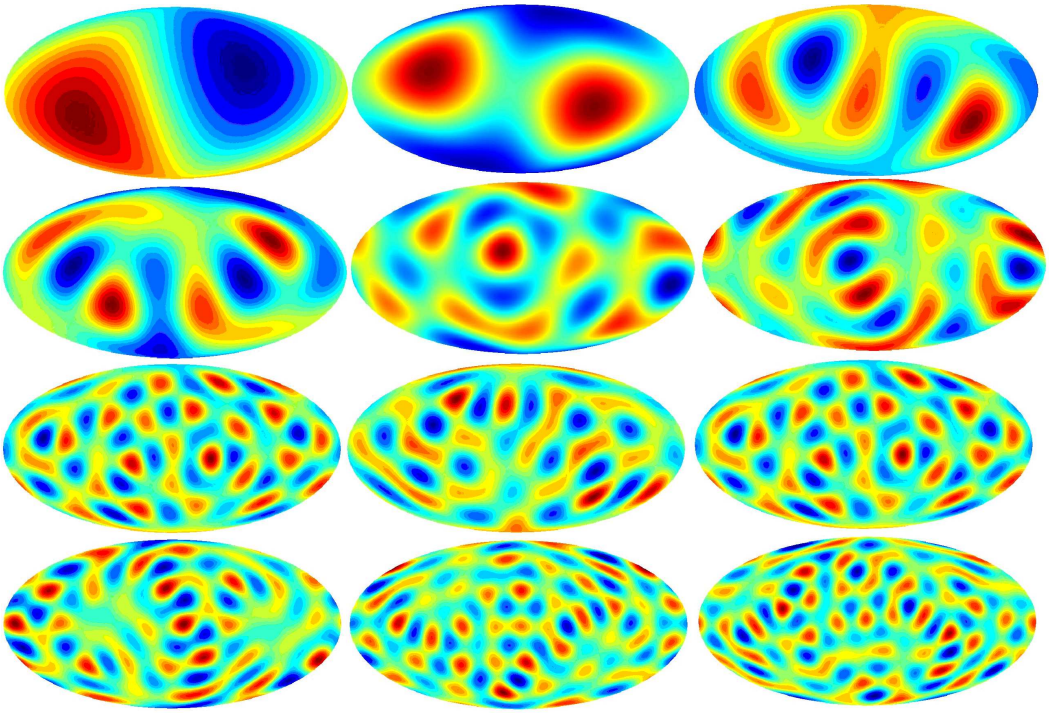


Figure 9: Randomly generated skies containing only a single multipole ℓ. Staring from top left: $\ell = 1$ (dipole), 2 (quadrupole), 3 (octopole), 4, 5, 6, 7, 8, 9, 10, 11, 12. Figure by Ville Heikkilä.

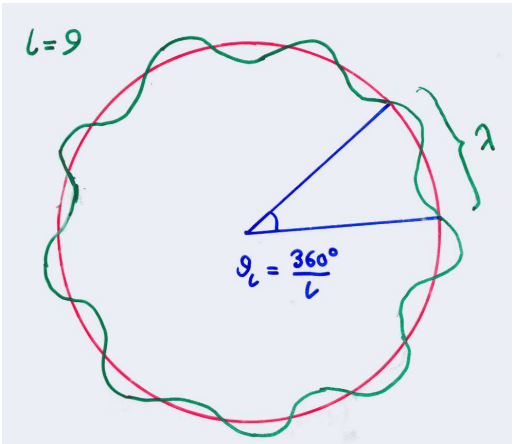


Figure 10: Rough correspondence between multipoles ℓ and angles.

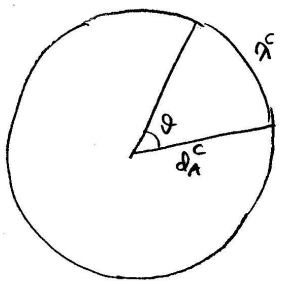


Figure 11: The comoving angular diameter distance relates the comoving size of an object and the angle at which we see it.

on the $t = t_{\rm dec}$ time slice. We want to obtain the multipole expansion of the values of this function on the last scattering sphere, by applying the expansion of the plane wave in terms of spherical harmonics (10.6). See figure 12. These are the values $f(x\hat{\boldsymbol{x}})$, where $x \equiv |\boldsymbol{x}|$ has a constant value, the (comoving) radius of this sphere. Thus

$$\begin{aligned} a_{\ell m} &= \int \mathrm{d}\Omega_x Y^*_{\ell m}(\hat{\boldsymbol{x}}) f(x\hat{\boldsymbol{x}}) \\ &= \sum_{\boldsymbol{k}} \int \mathrm{d}\Omega_x Y^*_{\ell m}(\hat{\boldsymbol{x}}) f_{\boldsymbol{k}} e^{i\boldsymbol{k}\cdot\boldsymbol{x}} \\ &= 4\pi \sum_{\boldsymbol{k}} \sum_{\ell' m'} \int \mathrm{d}\Omega_x f_{\boldsymbol{k}} Y^*_{\ell m}(\hat{\boldsymbol{x}}) i^{\ell'} j_{\ell'}(kx) Y_{\ell' m'}(\hat{\boldsymbol{x}}) Y^*_{\ell' m'}(\hat{\boldsymbol{k}}) \\ &= 4\pi i^\ell \sum_{\boldsymbol{k}} f_{\boldsymbol{k}} j_\ell(kx) Y^*_{\ell m}(\hat{\boldsymbol{k}}) \ , \end{aligned} \tag{10.22}$$

where we used the orthonormality of the spherical harmonics. The corresponding result for the Fourier transform $f(\boldsymbol{k})$ is

$$a_{\ell m} = \frac{4\pi i^\ell}{(2\pi)^{3/2}} \int \mathrm{d}^3 k f(\boldsymbol{k}) j_\ell(kx) Y^*_{\ell m}(\hat{\boldsymbol{k}}) \ . \tag{10.23}$$

The j_ℓ are oscillating functions with decreasing amplitude. For large values of ℓ the position of the first (and largest) maximum is near $kx = \ell$ (see figure 13). Thus the $a_{\ell m}$ pick a large contribution from the Fourier modes $\boldsymbol{k}$ for which

$$kx \sim \ell \ . \tag{10.24}$$

In a flat universe the comoving distance x (from our location to the sphere of last scattering) and the comoving angular diameter distance d_A^c are equal, so we can write this result as

$$k d_A^c \sim \ell \ . \tag{10.25}$$

The conclusion is that a given multipole ℓ acquires a contribution from modes with a range of wavenumbers, but most of the contribution comes from near the value given by (10.25). This concentration is tighter for larger ℓ. We will use equation (10.25) for qualitative purposes.

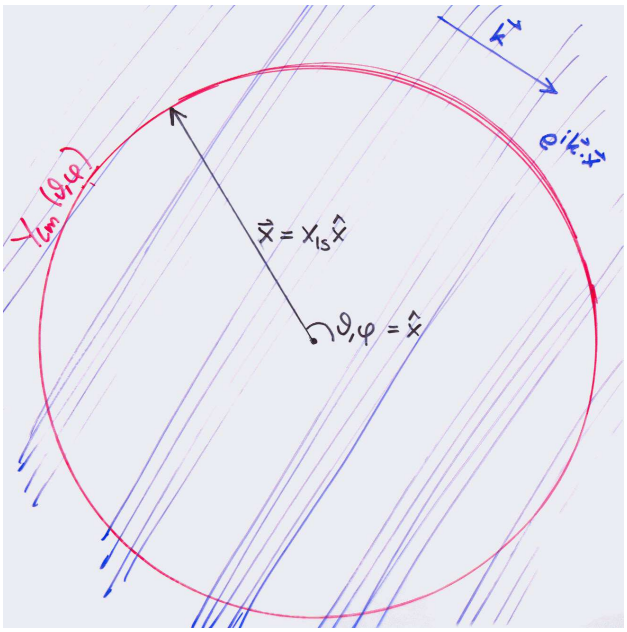


Figure 12: A plane wave intersecting the last scattering sphere.

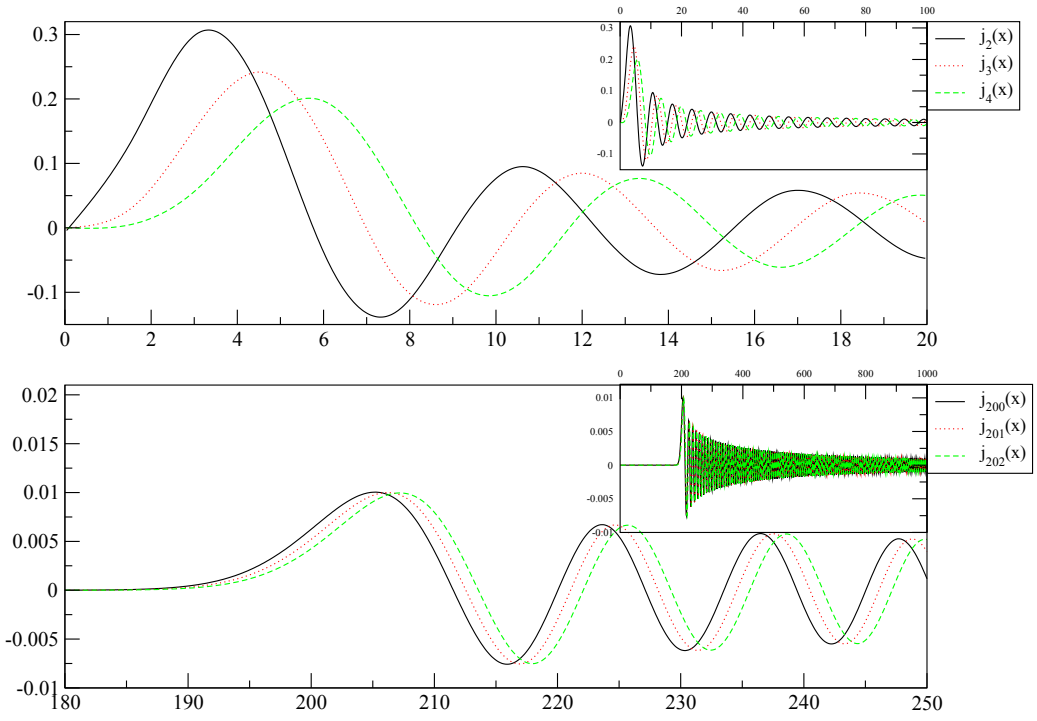


Figure 13: Spherical Bessel functions $j_\ell(x)$ for $\ell = 2$, 3, 4, 200, 201, and 202. Note how the first and largest peak is near $x = \ell$ (but to be precise, at a slightly larger value). Figure by R. Keskitalo.

10.4 Important distance scales on the last scattering surface

10.4.1 Angular diameter distance to the last scattering surface

In chapter 3 we derived the comoving angular diameter distance to redshift z in the FLRW model,

$$\begin{aligned} d_A^c(z) &= \frac{1}{\sqrt{-K}} \sinh\left(\sqrt{-K}\int_0^z \frac{\mathrm{d}z'}{H(z')}\right) \\ &= H_0^{-1}\int_{\frac{1}{1+z}}^1 \frac{\mathrm{d}a}{\sqrt{\Omega_0(a-a^2)-\Omega_{\Lambda 0}(a-a^4)+a^2}}\ , \end{aligned} \tag{10.26}$$

where the second line holds for an FLRW model that contains only matter and vacuum energy ($\Omega_0 = \Omega_{m0}+\Omega_{\Lambda 0}$). In the real universe, the contribution of radiation is small, since the radiation-dominated era ends early, when the universe is around 50 000 years old. Recall that $\Omega_0 - 1 = -\Omega_{K0} = K/H_0^2$. We are interested in the distance to the last scattering sphere, i.e. $d_A^c(z_{\rm dec})$, where $1 + z_{\rm dec} = 1091$.

In the simplest case of the spatially flat matter-dominated universe, $\Omega_{\Lambda 0} = 0$, $\Omega_{m0} = 1$, the integral gives

$$d_A^c(z_{\rm dec}) = H_0^{-1}\int_{\frac{1}{1+z_{\rm dec}}}^1 \frac{\mathrm{d}a}{\sqrt{a}} = 2H_0^{-1}\left(1-\frac{1}{\sqrt{1+z_{\rm dec}}}\right) = 1.94H_0^{-1} \approx 2H_0^{-1} \tag{10.27}$$

where the last approximation corresponds to ignoring the contribution from the lower limit.

We also consider two more general situations, of which the above is a special case.

a) Open universe with no dark energy, $\Omega_{\Lambda 0} = 0$ and $\Omega_{m0} = \Omega_0 < 1$. Now we have

$$\begin{aligned} d_A^c(z_{\rm dec}) &= \frac{H_0^{-1}}{\sqrt{1-\Omega_{m0}}} \sinh\left(\sqrt{1-\Omega_{m0}}\int_{\frac{1}{1+z}}^1 \frac{\mathrm{d}a}{\sqrt{(1-\Omega_{m0})a^2+\Omega_{m0}a}}\right) \\ &= \frac{H_0^{-1}}{\sqrt{1-\Omega_{m0}}} \sinh\left(\int_{\frac{1}{1+z}}^1 \frac{\mathrm{d}a}{\sqrt{a^2+\frac{\Omega_{m0}}{1-\Omega_{m0}}a}}\right) \\ &= \frac{H_0^{-1}}{\sqrt{1-\Omega_{m0}}} \sinh\left(2\ ,\mathrm{arsinh}\sqrt{\frac{1-\Omega_{m0}}{\Omega_{m0}}} - 2\ ,\mathrm{arsinh}\sqrt{\frac{1-\Omega_{m0}}{\Omega_{m0}}\frac{1}{1+z_{\rm dec}}}\right) \\ &\approx \frac{H_0^{-1}}{\sqrt{1-\Omega_{m0}}} \sinh\left(2\ ,\mathrm{arsinh}\sqrt{\frac{1-\Omega_{m0}}{\Omega_{m0}}}\right) \\ &= 2\frac{H_0^{-1}}{\Omega_{m0}}\ , \end{aligned} \tag{10.28}$$

where again the approximation ignores the contribution from the lower limit (i.e. it gives the comoving angular diameter distance to the horizon, $d_A^c(z = \infty)$). In the last step we used $\sinh 2x = 2\sinh x\cosh x = 2\sinh x\sqrt{1+\sinh^2 x}$. We show this result (together with the comoving proper distance $d_P^c(z = \infty)$) in figure 14.

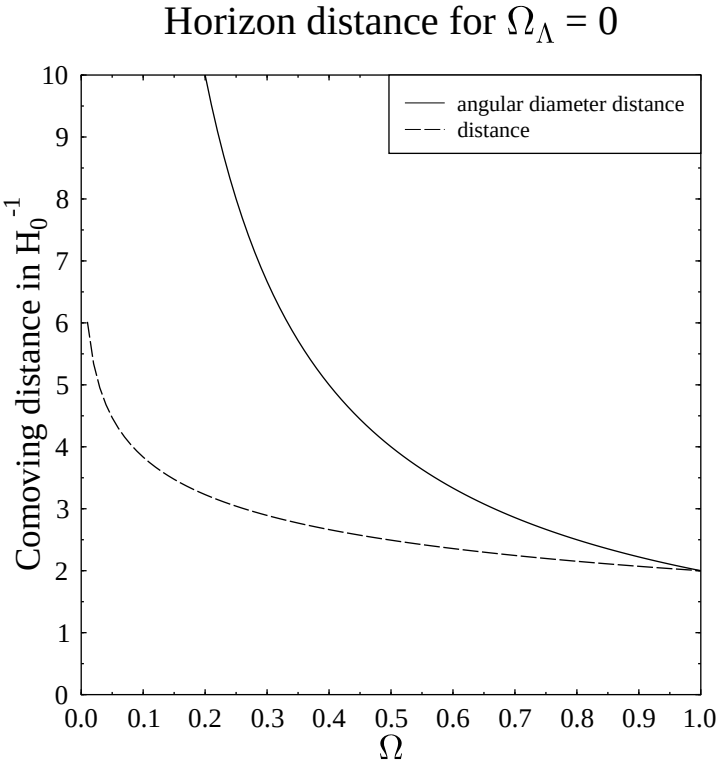


Figure 14: The comoving proper distance $d_P^c(z = \infty)$ (dashed) and the comoving angular diameter distance $d_A^c(z = \infty)$ (solid) to the horizon in matter-only open universe. The vertical axis is the distance in units of Hubble distance H_0^{-1} and the horizontal axis is the density parameter $\Omega_0 = \Omega_{m0}$. The distances to last scattering, $d_P^c(z_{\rm dec})$ and $d_A^c(z_{\rm dec})$, are a few per cent smaller.

b) Spatially flat universe with vacuum energy, $\Omega_\Lambda + \Omega_m = 1$. Here the integral does not give an elementary function, but for values close to the observed ones a reasonable approximation is

$$d_A^c(z_{\rm dec}) \approx \frac{2}{\Omega_m^{0.4}} H_0^{-1} \approx 3H_0^{-1} \ , \tag{10.29}$$

where the last approximate equality is for $\Omega_{m0} = 0.3$. The distance $d_A^c(z_{\rm dec})$ depends on the expansion history of the universe. For one, the longer it takes for the universe to cool from $T_{\rm dec}$ to T_0 (i.e. to expand by the factor $1 + z_{\rm dec}$), the longer distance the photons have time to travel. For spatially curved universes the angular diameter distance gets an additional effect from the geometry of the universe, which acts like a lens, making the CMB pattern at the last scattering sphere look smaller or larger (see figure 15).

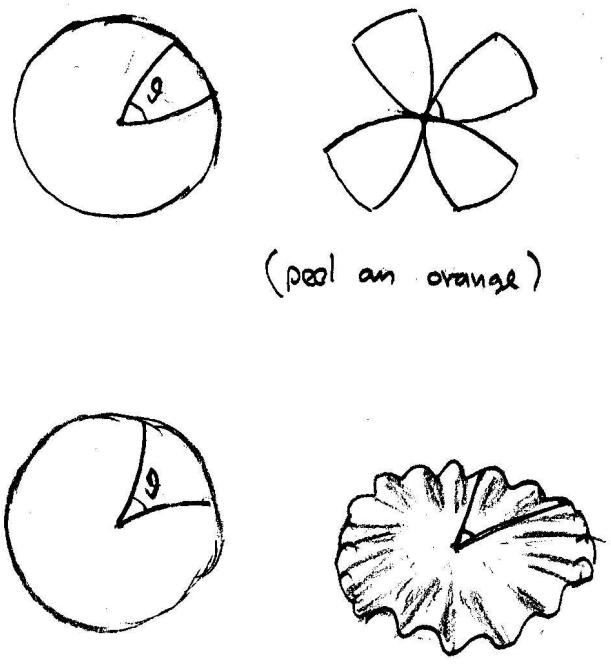


Figure 15: The geometry effect in a closed (top) or an open (bottom) universe affects the angle at which we see a structure of given size at the last scattering surface, and thus its angular diameter distance.

10.4.2 Decoupling scale and the matter-radiation equality scale

Sub-Hubble ($k \gg aH$) and super-Hubble ($k \ll aH$) scales behave differently. Thus we want to know which of the structures we see on the last scattering surface are sub-Hubble and which are super-Hubble at the time of last scattering. For that we need to know the comoving Hubble scale aH at $t_{\rm dec}$.

We make the approximation that neutrinos are massless. The physical radiation density today is then $\omega_r \equiv \Omega_{r0}h^2 = 4.18 \times 10^{-5}$, of which the photon contribution is $\omega_\gamma = 2.47 \times 10^{-5}$. We also make the approximation that the universe is completely

matter-dominated at $t_{\rm dec}$, i.e. we ignore the radiation contribution to the Friedmann equation at $t_{\rm dec}$. This is not an a very good approximation, since

$$\frac{\rho_m(t_{\rm dec})}{\rho_r(t_{\rm dec})} = \frac{\omega_m}{(1+z_{\rm dec})\omega_r} \approx 22\omega_m \approx 3.1 \ , \tag{10.30}$$

for $\omega_m = 0.14$. The curvature and (for most dark energy models, including vacuum energy) dark energy contributions are negligible at $t_{\rm dec}$. We thus have

$$H_{\rm dec}^2 \approx \frac{8\pi G}{3}\rho_m = \Omega_{m0}H_0^2(1+z_{\rm dec})^3 \ , \tag{10.31}$$

and the comoving Hubble scale is

$$k_{\rm dec}^{-1} \equiv (a_{\rm dec}H_{\rm dec})^{-1} = (1+z_{\rm dec})H_{\rm dec}^{-1} = (1+z_{\rm dec})^{-1/2}\frac{H_0^{-1}}{\sqrt{\Omega_{m0}}} = \frac{91{\rm Mpc}}{\sqrt{\omega_m}} \ , \tag{10.32}$$

where we have used $1+z_{\rm dec} = 1090$. The scale that enters at $t = t_{\rm dec}$ is thus

$$k_{\rm dec} = a_{\rm dec}H_{\rm dec} = (1+z_{\rm dec})^{1/2}\sqrt{\Omega_{m0}}H_0 \ , \tag{10.33}$$

and the corresponding multipole number on the last scattering sphere is

$$\ell_H \ \equiv \ k_{\rm dec}d_A^c \ = \ (1+z_{\rm dec})^{1/2}\sqrt{\Omega_{m0}} \times \left\{ \begin{array}{lll} 2/\Omega_{m0} & = & 66.0\,\Omega_{m0}^{-0.5} \approx 120 \quad (\Omega_\Lambda = 0) \\ 2/\Omega_{m0}^{0.4} & = & 66.0\,\Omega_{m0}^{0.1} \approx 74 \quad\ \ (\Omega_0 = 1) \ , \end{array} \right. \tag{10.34}$$

where the last equalities are for $\Omega_{m0} = 0.30$. The angle subtended by a half-wavelength π/k of this mode on the last scattering sphere is

$$\theta_H \equiv \frac{\pi}{\ell_H} = \frac{180^\circ}{\ell_H} = \left\{ \begin{array}{l} 2.7^\circ\,\Omega_{m0}^{0.5} \\ 2.7^\circ\,\Omega_{m0}^{-0.1} \ . \end{array} \right. \tag{10.35}$$

For the open model with $\Omega_{m0} = 0.3$, we get 1.5°, and for the spatially flat ΛCDM model with $\Omega_{m0} = 0.3$, we get 3°.

Another important scale is $k_{\rm eq}$, the scale that enters at matter-radiation equality time $t_{\rm eq}$, since the transfer function $T(k)$ bends at that point. Perturbations for scales $k \ll k_{\rm eq}$ essentially maintain their primordial spectrum, whereas scales $k \gg k_{\rm eq}$ have lost relative power between their Hubble entry and $t_{\rm eq}$. With a calculation similar to $k_{\rm dec}$ (taking into account that $\rho_{\rm tot}(t_{\rm eq}) = 2\rho_m(t_{\rm eq})$), we get

$$k_{\rm eq}^{-1} = (a_{\rm eq}H_{\rm eq})^{-1} \approx 14\omega_m^{-1}\ {\rm Mpc} \ . \tag{10.36}$$

For $\omega_m = 0.14$ we have $k_{\rm eq} = 100$ Mpc. The corresponding multipole number is

$$l_{\rm eq} = k_{\rm eq}d_A^c = 214\Omega_{m0}h \times \left\{ \begin{array}{lll} 2/\Omega_{m0} & = & 430h \approx 300 \quad\ \ (\Omega_\Lambda = 0) \\ 2/\Omega_{m0}^{0.4} & \approx & 430h\,\Omega_{m0}^{0.6} \approx 150 \quad (\Omega_0 = 1) \ , \end{array} \right. \tag{10.37}$$

where the last equalities are again for $\Omega_{m0} = 0.30$.

10.5 CMB anisotropy from perturbation theory

In the beginning of this chapter, we noted that the CMB temperature anisotropy can be split into two parts,

$$\left(\frac{\delta T}{T}\right)_{\rm obs} = \left(\frac{\delta T}{T}\right)_{\rm intr} + \left(\frac{\delta T}{T}\right)_{\rm jour} , \tag{10.38}$$

and that this separation depends on the chosen coordinates. The calculation requires more general relativity tools than we have, so we just give the result.

$$\begin{aligned}
\left(\frac{\delta T}{T}\right)_{\rm jour} &= -\int_{\rm dec}^{o} {\rm d}\Phi + \boldsymbol{v}_{\rm obs}\cdot\hat{\boldsymbol{n}} + \int_{\rm dec}^{o} {\rm d}t\left(\dot{\Phi}+\dot{\Psi}-\dot{h}_{ij}\hat{n}^i\hat{n}^j\right) \\
&= \Phi(t_{\rm dec},\boldsymbol{x}_{\rm ls}) - \Phi(t_0,\boldsymbol{0}) + \boldsymbol{v}_{\rm obs}\cdot\hat{\boldsymbol{n}} + \int_{\rm dec}^{o} {\rm d}t\left(\dot{\Phi}+\dot{\Psi}-\dot{h}_{ij}\hat{n}^i\hat{n}^j\right) \\
&\overset{\Psi\approx\Phi}{=} \Phi(t_{\rm dec},\boldsymbol{x}_{\rm ls}) - \Phi(t_0,\boldsymbol{0}) + \boldsymbol{v}_{\rm obs}\cdot\hat{\boldsymbol{n}} + 2\int_{\rm dec}^{o} {\rm d}t\dot{\Phi} - \hat{n}^i\hat{n}^j\int_{\rm dec}^{o}{\rm d}t\dot{h}_{ij} ,
\end{aligned} \tag{10.39}$$

where the integral is from $(t_{\rm dec},\boldsymbol{x}_{\rm ls})$ to $(t_0,\boldsymbol{0})$ along the path of the photon (a null geodesic) and $\hat{\boldsymbol{n}}$ is a unit vector pointing in the direction the observer is looking at. The observer's location has been chosen as the origin, $\boldsymbol{x}=\boldsymbol{0}$. The term $\boldsymbol{v}_{\rm obs}\cdot\hat{\boldsymbol{n}}$ is the Doppler effect from the observer's motion (assumed nonrelativistic, $|\boldsymbol{v}_{\rm obs}|\ll 1$), where $\boldsymbol{v}_{\rm obs}$ is the observer's velocity. The subscript ls in $\boldsymbol{x}_{\rm ls}$ indicates that $\boldsymbol{x}$ lies on the last scattering sphere. In the matter-dominated era the Newtonian potential remains constant in time, $\dot{\Phi}=0$, so there is a contribution from the integral only from epochs where the contributions of spatial curvature, radiation, or dark energy to the expansion of the universe cannot be neglected.[4]

We can understand the above result as follows. If the potential is constant in time, the blueshift the photon acquires when falling into a potential well is canceled by the redshift from climbing up the well. Thus the net redshift/blueshift caused by gravitational potential perturbations is just the difference between the values of Φ at the beginning and in the end. However, if the potential changes while the photon traverses the well, the cancellation is not exact, and the integral term accounts for this.

The value of the potential perturbation at the observing site, $\Phi(t_0,\boldsymbol{0})$ is the same for photons coming from all directions. Thus it does not contribute to the observed anisotropy. It just produces an overall shift in the observed average temperature. (Recall the discussion of the two ways of defining the mean temperature at the beginning of the chapter.) This is included in the observed value $T_0 = 2.725$ K, and we cannot separate it from the unperturbed value. We will thus ignore the monopole. As discussed, the observer motion $\boldsymbol{v}_{\rm obs}$ causes a (dominantly) dipole ($\ell=1$) pattern in the CMB anisotropy, from which it is difficult to disentangle the cosmological dipole on the last scattering sphere. Therefore the dipole is usually removed from the CMB map before analysing it for cosmological purposes. Accordingly, we also ignore this term. We will also not consider the effect of gravitational waves. Our

[4] This is peculiar to linear perturbation theory. In second and higher order perturbation theory we have $\dot{\Phi}\neq 0$ even in a spatially flat matter-dominated universe.

final result for the journey part is therefore

$$\left(\frac{\delta T}{T}\right)_{\rm jour} = \Phi(t_{\rm dec}, \boldsymbol{x}_{\rm ls}) + 2\int_{\rm dec}^{o} \dot{\Phi} {\rm d}t \ . \tag{10.40}$$

The other part, $\left(\frac{\delta T}{T}\right)_{\rm intr}$, comes from the local temperature perturbation at $t = t_{\rm dec}$ and the Doppler effect, $-\boldsymbol{v}\cdot\hat{\boldsymbol{n}}$, from the local (baryon+photon) fluid motion at that time. Since

$$\rho_\gamma = \frac{\pi^2}{15} T^4 \ , \tag{10.41}$$

the local temperature perturbation is directly related to the relative perturbation in the photon energy density,

$$\left(\frac{\delta T}{T}\right)_{\rm intr} = \frac{1}{4}\delta_\gamma - \boldsymbol{v}\cdot\hat{\boldsymbol{n}} \ . \tag{10.42}$$

We can now write the observed temperature anisotropy as

$$\left(\frac{\delta T}{T}\right)_{\rm obs} = \frac{1}{4}\delta_\gamma - \boldsymbol{v}\cdot\hat{\boldsymbol{n}} + \Phi(t_{\rm dec}, \boldsymbol{x}_{\rm ls}) + 2\int_{\rm dec}^{o} \dot{\Phi} {\rm d}t \ . \tag{10.43}$$

To make further progress we now

1. consider only adiabatic primordial perturbations and
2. make the (crude) approximation that the universe is already matter-dominated at $t = t_{\rm dec}$.

For adiabatic perturbations we have

$$\delta_b = \delta_c \equiv \delta_m = \frac{3}{4}\delta_\gamma \ . \tag{10.44}$$

The perturbations stay adiabatic only on super-Hubble scales. Once the perturbation has entered the Hubble radius, different physics begins to act on the different matter components, breaking the adiabatic relation between their density perturbations. In particular, the baryon-photon perturbation is affected by photon pressure, which damps its growth and causes it to oscillate, whereas the CDM perturbation is unaffected and keeps growing. Since the baryon and photon components see the same pressure, they evolve together and maintain their adiabatic relation until photon decoupling. Thus, after Hubble entry but before decoupling we have

$$\delta_c \neq \delta_b = \frac{3}{4}\delta_\gamma \ . \tag{10.45}$$

At decoupling, the equality holds for scales larger than the photon mean free path at $t_{\rm dec}$.

After decoupling, this connection between the photons and baryons is broken, and the baryon density perturbation begins to approach the CDM density perturbation,

$$\delta_c \leftarrow \delta_b \neq \frac{3}{4}\delta_\gamma \ . \tag{10.46}$$

We shall return to these issues when we discuss the shorter scales in sections 10.7 and 10.8. But let us first consider the scales which are still super-Hubble at $t_{\rm dec}$, so that (10.44) applies.

10.6 Large scales: Sachs–Wolfe part of the spectrum

Consider now the scales $k \ll k_{\rm dec}$, or $\ell \ll \ell_H$, which are still super-Hubble at decoupling. According to the adiabatic condition (10.44) we have

$$\frac{1}{4}\delta_\gamma = \frac{1}{3}\delta_m \approx \frac{1}{3}\delta \ , \tag{10.47}$$

where the latter (approximate) equality comes from taking the universe to be matter-dominated at $t_{\rm dec}$, so we can identify $\delta \approx \delta_m$. For these scales the Doppler effect from fluid motion is subdominant and we can ignore it. This can be seen from (9.19): Fourier transforming the equation we have $u^i \sim k^i\Phi/(a^2H)$. So (10.43) becomes

$$\left(\frac{\delta T}{T}\right)_{\rm obs} = \frac{1}{3}\delta + \Phi(t_{\rm dec}, \boldsymbol{x}_{\rm ls}) + 2\int_{\rm dec}^{o} \dot{\Phi}{\rm d}t \ . \tag{10.48}$$

On super-Hubble scales we have $\delta = -2\Phi$ and (10.48) becomes

$$\begin{aligned}\left(\frac{\delta T}{T}\right)_{\rm obs} &= -\frac{2}{3}\Phi(t_{\rm dec}, \boldsymbol{x}_{\rm ls}) + \Phi(t_{\rm dec}, \boldsymbol{x}_{\rm ls}) + 2\int_{\rm dec}^{o} \dot{\Phi}{\rm d}t \\ &= \frac{1}{3}\Phi(t_{\rm dec}, \boldsymbol{x}_{\rm ls}) + 2\int_{\rm dec}^{o} \dot{\Phi}{\rm d}t \ .\end{aligned} \tag{10.49}$$

This part of the CMB anisotropy is called the *Sachs–Wolfe effect*. The first part, $\frac{1}{3}\Phi(t_{\rm dec}, \boldsymbol{x}_{\rm ls})$, is called the *ordinary* Sachs–Wolfe effect, and the second part, $2\int \dot{\Phi}{\rm d}t$, is called the *integrated Sachs-Wolfe effect* (ISW), since it involves integrating along the line of sight. There are two contributions to the integrated Sachs–Wolfe effect: the *early Sachs–Wolfe effect* and the *late Sachs–Wolfe effect*. The first is caused by radiation at last scattering. In our approximation where we assume that the universe is completely matter-dominated at $t = t_{\rm dec}$, this term is absent. When dark energy becomes important at times close to today, Φ starts to evolve again, which leads to the late ISW effect, which shows up as a rise in the smallest ℓ of the angular power spectrum C_ℓ. However, it is difficult to detect this effect due to the large cosmic variance at small ℓ. The late ISW effect also leads to a correlation between the CMB anisotropies and the galaxy distribution, which makes it easier to detect its presence. The late ISW effect has been detected this way, by cross-correlating the CMB and large-scale structure. Also, with the Planck data, it has been detected for the first time purely from the CMB by using the correlation of the ISW effect and *gravitational lensing* of the CMB (the latter is also correlated with large-scale structure). We will not discuss gravitational lensing. We will now for a while ignore the ISW, which for $\ell \ll \ell_H$ is expected to be smaller than the ordinary Sachs–Wolfe effect.

10.6.1 Angular power spectrum from the ordinary Sachs–Wolfe effect

Let us now calculate the contribution from the ordinary Sachs–Wolfe effect,

$$\left(\frac{\delta T}{T}\right)_{\rm SW} = \frac{1}{3}\Phi(t_{\rm dec}, \boldsymbol{x}_{\rm ls}) \ , \tag{10.50}$$

to the angular power spectrum C_ℓ. This is the dominant effect for $\ell \ll \ell_H$.

Since Φ is evaluated at the last scattering sphere, we have from (10.22)

$$a_{\ell m} = 4\pi i^\ell \sum_{\boldsymbol{k}} \frac{1}{3} \Phi_{\boldsymbol{k}} j_\ell(kx) Y^*_{\ell m}(\hat{\boldsymbol{k}}) \ , \tag{10.51}$$

In the matter-dominated era,

$$\Phi = -\frac{3}{5}\mathcal{R} \ , \tag{10.52}$$

so

$$a_{\ell m} = -\frac{4\pi}{5} i^\ell \sum_{\boldsymbol{k}} \mathcal{R}_{\boldsymbol{k}} j_\ell(kx) Y^*_{\ell m}(\hat{\boldsymbol{k}}) \ . \tag{10.53}$$

The coefficient $a_{\ell m}$ is thus a linear combination of the independent random variables $\mathcal{R}_{\boldsymbol{k}}$, i.e. it is of the form

$$\sum_{\boldsymbol{k}} b_{\boldsymbol{k}} \mathcal{R}_{\boldsymbol{k}} \ , \tag{10.54}$$

For any such linear combination, the expectation value of its absolute value squared is

$$\begin{aligned} \left\langle \left| \sum_{\boldsymbol{k}} b_{\boldsymbol{k}} \mathcal{R}_{\boldsymbol{k}} \right|^2 \right\rangle &= \sum_{\boldsymbol{k}} \sum_{\boldsymbol{k}'} b_{\boldsymbol{k}} b^*_{\boldsymbol{k}'} \left\langle \mathcal{R}_{\boldsymbol{k}} \mathcal{R}^*_{\boldsymbol{k}'} \right\rangle \\ &= \left(\frac{2\pi}{L} \right)^3 \sum_{\boldsymbol{k}} \frac{1}{4\pi k^3} \mathcal{P}_{\mathcal{R}}(k) \left| b_{\boldsymbol{k}} \right|^2 \ , \end{aligned} \tag{10.55}$$

where we used

$$\left\langle \mathcal{R}_{\boldsymbol{k}} \mathcal{R}^*_{\boldsymbol{k}'} \right\rangle = \delta_{\boldsymbol{k}\boldsymbol{k}'} \left(\frac{2\pi}{L} \right)^3 \frac{1}{4\pi k^3} \mathcal{P}_{\mathcal{R}}(k) \ , \tag{10.56}$$

i.e. the independence of the random variables $\mathcal{R}_{\boldsymbol{k}}$ and the definition of the power spectrum $\mathcal{P}(k)$. Thus

$$\begin{aligned} C_\ell &= \frac{1}{2\ell+1} \sum_m \langle |a_{\ell m}|^2 \rangle \\ &= \frac{16\pi^2}{25} \frac{1}{2\ell+1} \sum_m \left(\frac{2\pi}{L} \right)^3 \sum_{\boldsymbol{k}} \frac{1}{4\pi k^3} \mathcal{P}_{\mathcal{R}}(k) j_\ell(kx)^2 |Y^*_{\ell m}(\hat{\boldsymbol{k}})|^2 \\ &= \frac{1}{25} \left(\frac{2\pi}{L} \right)^3 \sum_{\boldsymbol{k}} \frac{1}{k^3} \mathcal{P}_{\mathcal{R}}(k) j_\ell(kx)^2 \ . \end{aligned} \tag{10.57}$$

(Although all $\langle |a_{\ell m}|^2 \rangle$ are equal for the same ℓ, we used the sum over m in order to apply (10.5).) Replacing the sum with an integral, we get

$$C_\ell = \frac{1}{25} \int \frac{\mathrm{d}^3 k}{k^3} \mathcal{P}_{\mathcal{R}}(k) j_\ell(kx)^2 = \frac{4\pi}{25} \int_0^\infty \frac{\mathrm{d}k}{k} \mathcal{P}_{\mathcal{R}}(k) j_\ell(kx)^2 \ , \tag{10.58}$$

which is the final result for an arbitrary primordial power spectrum $\mathcal{P}_{\mathcal{R}}(k)$.

The integral can be done for a power-law power spectrum, $\mathcal{P}_\mathcal{R}(k) = A^2(k/k_*)^{n_s-1}$. In particular, for a scale-invariant primordial power spectrum ($n_s = 1$),

$$\mathcal{P}_\mathcal{R}(k) = \text{constant} = A^2 \ , \tag{10.59}$$

we have

$$C_\ell = A^2 \frac{4\pi}{25} \int_0^\infty \frac{\mathrm{d}k}{k} j_\ell(kx)^2 = \frac{A^2}{25} \frac{2\pi}{\ell(\ell+1)} \ , \tag{10.60}$$

since

$$\int_0^\infty \frac{\mathrm{d}k}{k} j_\ell(kx)^2 = \frac{1}{2\ell(\ell+1)} \ . \tag{10.61}$$

We can write this as

$$\frac{\ell(\ell+1)}{2\pi} C_\ell = \frac{A^2}{25} = \text{constant (independent of } \ell) \ . \tag{10.62}$$

The reason why the angular power spectrum is customarily plotted as $\ell(\ell+1)C_\ell$ is that it makes the Sachs–Wolfe part of the C_ℓ flat for a scale-invariant primordial power spectrum $\mathcal{P}_\mathcal{R}(k)$.

Present data shows that the spectrum has a small red tilt, $n = 0.9649 \pm 0.0042$ [2] (this number assumes the ΛCDM model; in more complicated models, the results can be slightly different), as expected from many inflationary models. Since the spectrum is close to scale-invariant, determining the spectral index requires observations over a range of scales. However, it is possible to determine the overall amplitude just from the few lowest multipoles, known as the *Sachs–Wolfe plateau*. The COBE satellite saw only up to about $\ell = 25$, so the COBE data in figure 1 is completely in this region. The amplitude is

$$\frac{\ell(\ell+1)}{2\pi} \widehat{C}_\ell \approx 10^{-10} \ , \tag{10.63}$$

coresponding to the amplitude of the primordial power spectrum

$$\mathcal{P}_\mathcal{R}(k) = A^2 \approx 2 - 1 \times 10^{-9} = \left(4.6 \times 10^{-5}\right)^2 \ . \tag{10.64}$$

We already used this result (confirmed after COBE by other experiments) in chapter 8 as a constraint on the energy scale of inflation. Nowadays, the detailed structure of the anisotropies has been measured: data from Planck is shown in figure 8. Let us now discuss how the structure of peaks and troughs is generated.

10.7 Acoustic oscillations

Consider now the scales $k \gg k_{\mathrm{dec}}$, or $\ell \gg \ell_H$, which are sub-Hubble at decoupling. The observed temperature anisotropy is, from (10.43)

$$\left(\frac{\delta T}{T}\right)_{\mathrm{obs}} = \frac{1}{4}\delta_\gamma(t_{\mathrm{dec}}, \boldsymbol{x}_{\mathrm{ls}}) + \Phi(t_{\mathrm{dec}}, \boldsymbol{x}_{\mathrm{ls}}) - \boldsymbol{v} \cdot \hat{\boldsymbol{n}}(t_{\mathrm{dec}}, \boldsymbol{x}_{\mathrm{ls}}) + 2\int_{\mathrm{dec}}^{o} \dot{\Phi} \mathrm{d}t \ . \tag{10.65}$$

We concentrate on the first three terms, which are determined by the situation at the point $(t_{\mathrm{dec}}, \boldsymbol{x}_{\mathrm{ls}})$ that we are looking at on the last scattering sphere.

Before decoupling the photons are tightly coupled to the baryons. The perturbations in the baryon-photon fluid oscillate, whereas CDM perturbations grow (logarithmically during the radiation-dominated epoch, and then linearly, $\propto a$, during the matter-dominated epoch). Therefore CDM perturbations begin to dominate the total density perturbation $\delta\rho$ and thus also Φ already before the universe becomes matter-dominated and CDM begins to dominate the background energy density. Thus we can make the approximation that Φ is given by the CDM perturbation. The baryon-photon fluid oscillates in these potential wells caused by the CDM. The potential Φ evolves at first but then becomes constant as the universe becomes matter-dominated.

We will not do a full calculation of the $\delta_{b\gamma}$ oscillations in the expanding universe. We instead give, without derivation, the equation for the density contrast of fluid component i in the case when we neglect expansion:

$$\ddot{\delta}_{\boldsymbol{k}i} + k^2 \left[c_s^2 \delta_{\boldsymbol{k}i} + (1+w_i)\Phi_{\boldsymbol{k}}\right] = 0 \ . \tag{10.66}$$

In the present application the fluid component ρ_i is the baryon-photon fluid $\rho_{b\gamma}$ and the gravitational potential Φ is caused by the CDM. Before decoupling, the adiabatic relation $\delta_b = \frac{3}{4}\delta_\gamma$ still holds between photons and baryons, and we have the adiabatic relation between pressure and density perturbations,

$$\delta p_{b\gamma} = c_s^2 \delta\rho_{b\gamma} \ , \tag{10.67}$$

so the sound speed of the fluid is given by

$$c_s^2 = \frac{\delta p_{b\gamma}}{\delta\rho_{b\gamma}} \approx \frac{\delta p_\gamma}{\delta\rho_{b\gamma}} = \frac{1}{3}\frac{\delta\rho_\gamma}{\delta\rho_\gamma + \delta\rho_b} = \frac{1}{3}\frac{\bar{\rho}_\gamma\delta_\gamma}{\bar{\rho}_\gamma\delta_\gamma + \bar{\rho}_b\delta_b} = \frac{1}{3}\frac{1}{1+\frac{3}{4}\frac{\bar{\rho}_b}{\bar{\rho}_\gamma}} \equiv \frac{1}{3}\frac{1}{1+R} \ , \tag{10.68}$$

where we defined

$$R \equiv \frac{3}{4}\frac{\bar{\rho}_b}{\bar{\rho}_\gamma} \ . \tag{10.69}$$

We can now write the perturbation equation (10.66) for the baryon-photon fluid as

$$\ddot{\delta}_{b\gamma\boldsymbol{k}} + k^2 \left[c_s^2 \delta_{b\gamma\boldsymbol{k}} + (1+w_{b\gamma})\Phi_{\boldsymbol{k}}\right] = 0 \ . \tag{10.70}$$

The baryon-photon fluid equation of state is

$$w_{b\gamma} \equiv \frac{\bar{p}_{b\gamma}}{\bar{\rho}_{b\gamma}} = \frac{\frac{1}{3}\bar{\rho}_\gamma}{\bar{\rho}_\gamma + \bar{\rho}_b} = \frac{1}{3}\frac{1}{1+\frac{4}{3}R} \ , \tag{10.71}$$

We can therefore write (10.70) as

$$\ddot{\delta}_{b\gamma\boldsymbol{k}} + k^2 \left[\frac{1}{3}\frac{1}{1+R}\delta_{b\gamma\boldsymbol{k}} + \frac{\frac{4}{3}(1+R)}{1+\frac{4}{3}R}\Phi_{\boldsymbol{k}}\right] = 0 \ . \tag{10.72}$$

We introduce the notation[5]

$$\Theta_0 \equiv \frac{1}{4}\delta_\gamma \ , \tag{10.73}$$

[5]The subscript 0 refers to the monopole ($\ell = 0$) of the local photon distribution. Likewise, the dipole ($\ell = 1$) of the local photon distribution corresponds to the velocity of the photon fluid, $\Theta_1 \equiv v_\gamma/3$.

which gives the perturbation in the photons, not in the baryon-photon fluid. The two are related by

$$\delta_{b\gamma} = \frac{\delta\rho_{b\gamma}}{\bar{\rho}_{b\gamma}} = \frac{\delta\rho_\gamma + \delta\rho_b}{\bar{\rho}_\gamma + \bar{\rho}_b} = \frac{\bar{\rho}_\gamma\delta_\gamma + \bar{\rho}_b\delta_b}{\bar{\rho}_\gamma + \bar{\rho}_b} = \frac{1+R}{1+\frac{4}{3}R}\delta_\gamma \ . \tag{10.74}$$

Thus we can write (10.70) as

$$\ddot{\delta}_{\gamma\boldsymbol{k}} + k^2\left[\frac{1}{3}\frac{1}{1+R}\delta_{\gamma\boldsymbol{k}} + \frac{4}{3}\Phi_{\boldsymbol{k}}\right] = 0 \ , \tag{10.75}$$

or

$$\ddot{\Theta}_{0\boldsymbol{k}} + k^2\left[\frac{1}{3}\frac{1}{1+R}\Theta_{0\boldsymbol{k}} + \frac{1}{3}\Phi_{\boldsymbol{k}}\right] = 0 \ . \tag{10.76}$$

or

$$\ddot{\Theta}_{0\boldsymbol{k}} + c_s^2k^2\left[\Theta_{0\boldsymbol{k}} + (1+R)\Phi_{\boldsymbol{k}}\right] = 0 \ , \tag{10.77}$$

If we now take R and Φ_k to be constant, this is the harmonic oscillator equation for the quantity $\Theta_{0\boldsymbol{k}} + (1+R)\Phi_{\boldsymbol{k}}$ with the general solution

$$\Theta_{0\boldsymbol{k}} + (1+R)\Phi_{\boldsymbol{k}} = A_{\boldsymbol{k}}\cos(c_skt) + B_{\boldsymbol{k}}\sin(c_skt) \ , \tag{10.78}$$

or

$$\Theta_{0\boldsymbol{k}} + \Phi_{\boldsymbol{k}} = -R\Phi_{\boldsymbol{k}} + A_{\boldsymbol{k}}\cos(c_skt) + B_{\boldsymbol{k}}\sin(c_skt) \ . \tag{10.79}$$

We are interested in the quantity $\Theta_0 + \Phi = \frac{1}{4}\delta_\gamma + \Phi$, called the *effective temperature perturbation*, since this is the combination that appears in (10.65). It is the local temperature perturbation minus the redshift that photons undergo when climbing from the potential well of the perturbation (negative Φ for a CDM overdensity). We see that this quantity oscillates in time, and the effect of baryons (via R) is to shift the equilibrium point of the oscillation by $-R\Phi_{\boldsymbol{k}}$.

In the preceding we ignored the expansion of the universe. Expansion affects the result in several ways. For example, c_s, $w_{b\gamma}$, and R change with time. The potential Φ also evolves, especially at early times when radiation dominates the expansion. However, the qualitative result of an oscillation of $\Theta_0 + \Phi$, and the shift of its equilibrium point by baryons, remains. Time t in the solution (10.79) is replaced by conformal time η, and since c_s changes with time, $c_s\eta$ is replaced by

$$r_s^c(t) \equiv \int_0^\eta c_s\mathrm{d}\eta = \int_0^t \frac{c_s(t)}{a(t)}\mathrm{d}t \ . \tag{10.80}$$

We call this quantity $r_s^c(t)$ the *comoving sound horizon* at time t, since it gives the comoving distance sound waves have travelled to time t.

The relative weight of the cosine and sine solutions (i.e. the constants $A_{\boldsymbol{k}}$ and $B_{\boldsymbol{k}}$ in (10.78) depends on the initial conditions. The initial conditions are determined on super-Hubble scales, where the present discussion does not really apply. However, using the super-Hubble initial conditions gives the correct qualitative result for the phase of the oscillation.

We had that for adiabatic primordial perturbations, initially $\Phi = -\frac{3}{5}\mathcal{R}$ and $\frac{1}{4}\delta_\gamma = -\frac{2}{3}\Phi = \frac{2}{5}\mathcal{R}$, giving the initial condition $\Theta_0 + \Phi = \frac{1}{3}\Phi = -\frac{1}{5}\mathcal{R} =$ constant (At these early times $R \ll 1$, so we can drop the factor $1 + R$.) Thus adiabatic primordial perturbations correspond essentially to the cosine solution, as it approaches a constant for small values of the argument. There are effects at the Hubble scale which affect the amplitude of the oscillations –the main effect being the decay of Φ as it enters the Hubble radius– so we can't use the preceding discussion to determine the exact amplitude, but we get the right result about the initial phase of the $\Theta_0 + \Phi$ oscillations.

Thus we have that, qualitatively, the effective temperature behaves at sub-Hubble scales as

$$\Theta_{0\boldsymbol{k}} + (1+R)\Phi_{\boldsymbol{k}} \propto \cos[kr_s^c(t)] \ , \tag{10.81}$$

Consider a region where the primordial curvature perturbation $\mathcal{R}$ is positive. It initially has an overdensity (as we assume perturbations are adiabatic, this applies to all components: photons, baryons, CDM, and neutrinos) and a negative gravitational potential Φ. For the scales of interest for CMB anisotropy, the potential stays negative, since the CDM begins to dominate the potential early enough and the CDM perturbations do not oscillate, they just grow. The oscillating quantity, the effective temperature perturbation $\Theta_0 + \Phi$, begins with a negative value. After half an oscillation period it is at its positive extreme value. This increase of $\Theta_0 + \Phi$ corresponds to an increase in δ_γ; from its initial positive value it has grown to a larger positive value. Thus the oscillation begins by the initially overdense baryon-photon fluid element falling deeper into the potential well, and reaching maximum compression after half a period. After this maximum compression the photon pressure pushes the baryon-photon fluid out from the potential well, and after a full period, the fluid reaches its maximum decompression in the potential well. Since the potential Φ has meanwhile decayed (Hubble entry and the resulting potential decay always happens during the first oscillation period, since the sound horizon and the Hubble length are close to each other, as the sound speed is close to the speed of light), the decompression does not bring the $\delta_{b\gamma}$ back to its initial value (which was overdense), but the photon-baryon fluid actually becomes underdense in the potential well (and overdense in the neighbouring potential hill). And so the oscillation goes on until photon decoupling.

These standing waves are called *acoustic oscillations*. See figure 16. Because of the potential decay at Hubble entry, the amplitude of the oscillation is larger than Φ, and thus also Θ_0 changes sign in the oscillation.

These oscillations end at photon decoupling, when the photons are liberated. The CMB shows these standing waves as a snapshot[6] at their final moment $t = t_{\rm dec}$.

At photon decoupling we have

$$\Theta_{0\boldsymbol{k}} + (1+R)\Phi_{\boldsymbol{k}} \propto \cos[kr_s^c(t_{\rm dec})] \ . \tag{10.82}$$

At this moment the oscillations for the scales k for which

$$kr_s^c(t_{\rm dec}) = n\pi \tag{10.83}$$

[6]Actually, photon decoupling takes quite a long time. Therefore this "snapshot" has a rather long exposure time causing it to be blurred. This prevents us from seeing very small scales in the CMB anisotropy.

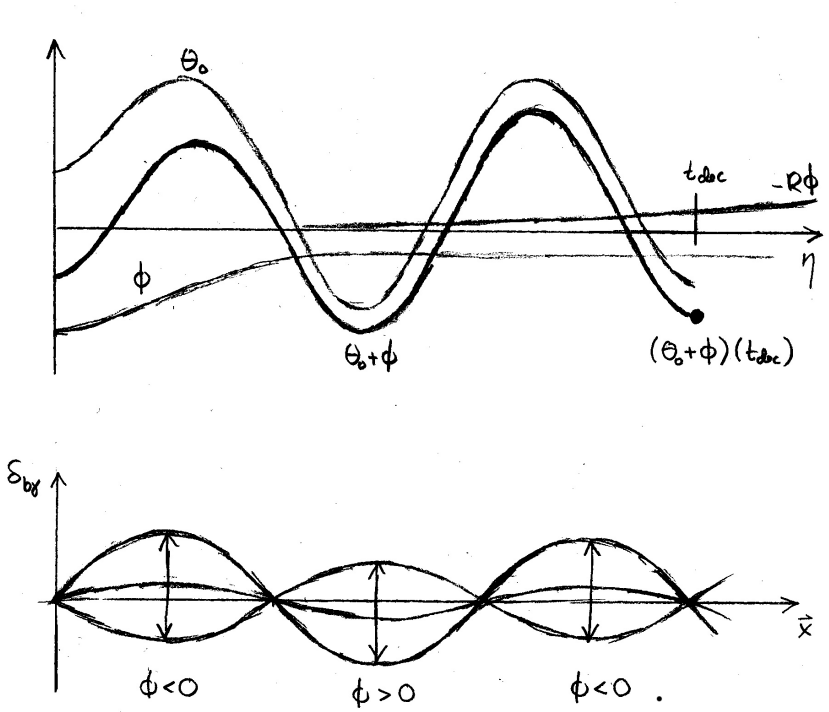


Figure 16: Acoustic oscillations. The top panel shows the time evolution of $\Theta_{0\boldsymbol{k}}$, $\Phi_{\boldsymbol{k}}$, and the effective temperature $\Theta_{0\boldsymbol{k}} + \Phi_{\boldsymbol{k}}$. The Fourier mode shown corresponds to the fourth acoustic peak of the C_ℓ spectrum. The bottom panel shows $\delta_{b\gamma}(\boldsymbol{x})$ for one Fourier mode as a function of position at various times (maximum compression, equilibrium level, maximum decompression).

($n = 1, 2, 3, \ldots$) are at their extreme values (maximum compression or maximum decompression). Therefore we see strong structure in the CMB anisotropy at the multipoles

$$\ell = k d_A^c(t_{\rm dec}) = n\pi \frac{d_A^c(t_{\rm dec})}{r_s^c(t_{\rm dec})} \equiv n\ell_A \tag{10.84}$$

corresponding to these scales. Here

$$\ell_A \equiv \pi \frac{d_A^c(t_{\rm dec})}{r_s^c(t_{\rm dec})} \equiv \frac{\pi}{\theta_s} \tag{10.85}$$

is the *acoustic scale* in multipole space and

$$\theta_s \equiv \frac{r_s^c(t_{\rm dec})}{d_A^c(t_{\rm dec})} \tag{10.86}$$

is the *sound horizon angle*, i.e. the angle at which we see the sound horizon on the last scattering surface. This is the CMB anisotropy quantity determined with the best precision from the data. From the Planck data alone and assuming the ΛCDM model, we get $100\theta_s = 1.04092 \pm 0.00031$, or $\theta_s = 0.596403 \pm 0.00018°$, a precision of 0.03% [2]. This quantity is also rather easy to determine model-independently, because the location of the acoustic peaks in multipole space is very well determined from observation. Even with the older WMAP data and ACBAR ground-based CMB experiment data we get, without assuming ΛCDM, the model-independent value $\theta_s = 0.593° \pm 0.001°$, a precision of 0.3% [3].

Because of these acoustic oscillations, the CMB angular power spectrum C_ℓ has a structure of *acoustic peaks* on sub-Hubble scales. The centers of these peaks are located approximately at $\ell_n \approx n\ell_A$. An exact calculation shows that they actually lie at somewhat smaller ℓ due to a number of effects. The separation of neighbouring peaks is closer to ℓ_A than the positions of the peaks are to $n\ell_A$.

These acoustic oscillations are related to the motion of the baryon-photon fluid. When the oscillation of one Fourier mode is at its extreme, e.g. at the maximal compression in the potential well, the fluid is momentarily at rest, but then it begins flowing out of the well until it reaches the other extreme, maximal decompression. Therefore those Fourier modes $\boldsymbol{k}$ that have the maximum effect on the CMB anisotropy via the $\frac{1}{4}\delta_\gamma(t_{\rm dec}, \boldsymbol{x}_{\rm ls}) + \Phi(t_{\rm dec}, \boldsymbol{x}_{\rm ls})$ term (the effective temperature effect) in (10.65) have the minimum effect via the $-\boldsymbol{v}\cdot\hat{\boldsymbol{n}}(t_{\rm dec}, \boldsymbol{x}_{\rm ls})$ term (the Doppler effect) and vice versa. Therefore the Doppler effect also contributes a peak structure to the C_ℓ spectrum, but its peaks are in the locations where the effective temperature contribution has troughs.

The Doppler effect is subdominant to the effective temperature effect, and therefore the peak positions in the C_ℓ spectrum is determined by the effective temperature effect according to (10.84). The Doppler effect just partially fills the troughs between the peaks, weakening the peak structure of C_ℓ. See figure 19. The calculation involves some approximations which allow the description of C_ℓ as just a sum of these contributions, and is not as accurate as a full calculation using e.g. the COSMOMC code[7].

Figure 17 shows the values of the effective temperature perturbation $\Theta_0 + \Phi$ (as well as Θ_0 and Φ separately) and the magnitude of the velocity perturbation ($\Theta_1 \sim v/3$) at $t_{\rm dec}$ as a function of the scale k. This is a result of a numerical calculation which includes the effect of the expansion of the universe, but not diffusion damping.

10.8 Diffusion damping

For small enough scales photon diffusion and the finite thickness of the last scattering surface ($\sim$ the photon mean free path just before last scattering) smooth out the photon distribution and the CMB anisotropy. This effect is called diffusion damping or *Silk damping*. It is characterised by the damping scale k_D^{-1}, which is the distance that photons have travelled up to last scattering. The photon density and velocity perturbations at scale k are damped at $t_{\rm dec}$ by

$$e^{-k^2/k_D^2} \ , \tag{10.87}$$

and the C_ℓ spectrum is damped as

$$e^{-\ell^2/\ell_D^2} \ . \tag{10.88}$$

We can estimate k_D and ℓ_D as follows (see [4] page 129 for more details, or [5] page 169 for even more details). Before decoupling photons scatter from the electrons in the plasma. The typical time between collisions (i.e. photon mean free path) at time t is $\lambda_\gamma = t_c(t) = \Gamma^{-1} = (n_e(t)\sigma_T)^{-1}$, where $\sigma_T = \frac{8\pi}{3}\frac{\alpha^2}{m_e^2}$ is the Thomson cross-section. The free electron density depends on the ionisation fraction x (see section

[7] COSMOMC is a publicly available code for precise calculation of the C_ℓ spectrum. See https://cosmologist.info/cosmomc/

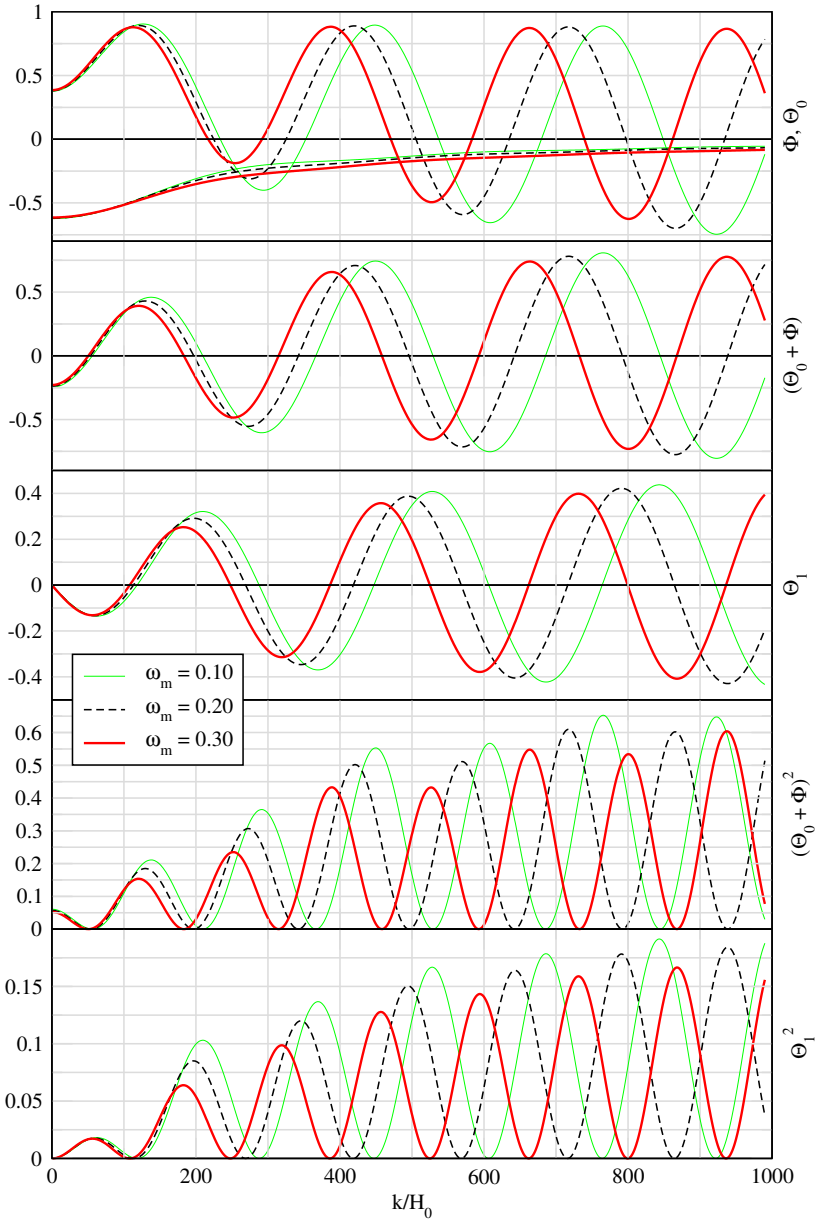


Figure 17: Values of oscillating quantities (normalised to initial value $\mathcal{R}_{\boldsymbol{k}} = 1$) at the time of decoupling as a function of the scale k, for three different values of ω_m, and for $\omega_b = 0.01$. Θ_1 represents the velocity perturbation. The effect of diffusion damping is neglected. Figure and calculation by R. Keskitalo.

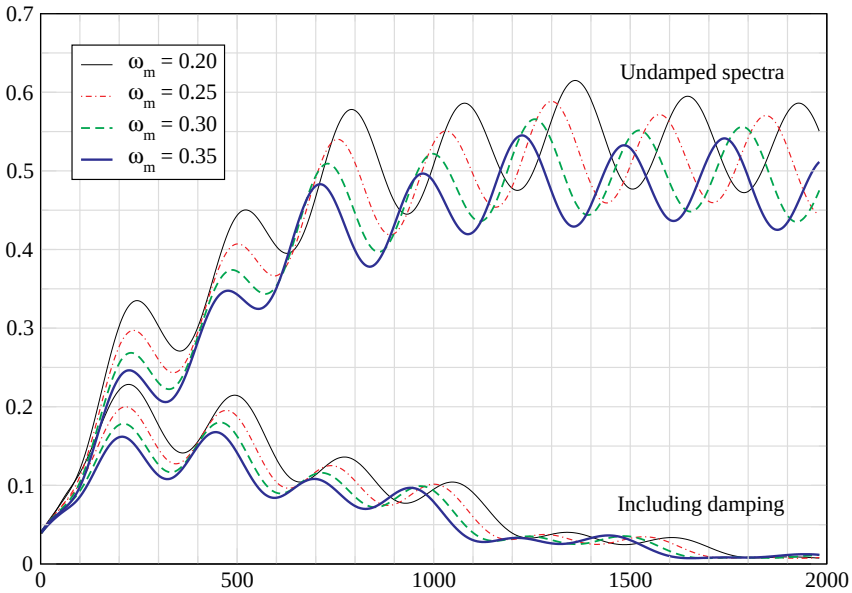


Figure 18: The angular power spectrum C_ℓ, calculated both with and without the effect of diffusion damping. The spectrum is given for four different values of ω_m, with $\omega_b = 0.01$. (This is about half the real value, so $\ell_D < 1500$ and the damping is quite strong.) Figure and calculation by R. Keskitalo.

4.11). For simplicity, we take $x = 1$. (In fact, the ionisation fraction drops, and t_c grows, rapidly during decoupling.) The photon direction changes randomly at each collision and independently of the previous collision, so photons undergo a random walk with uncorrelated steps. The number of steps the photons has taken up to time t is $N = t/t_c$ (taking t_c to be constant for simplicity), and the total distance it has travelled at decoupling is

$$d_D = \sqrt{N} t_c = \sqrt{t_{\rm dec} t_c} \approx 14 \text{ kpc} , \tag{10.89}$$

where we have put in $t_{\rm dec} = 380\ 000$ yr, $t_c = t_c(t_{\rm dec})$ and used $T_{\rm dec} = 3000$ K, $\eta = 6 \times 10^{-10}$. The comoving diffusion wavenumber is given by

$$k_D^{-1} = (1 + z_{\rm dec}) d_D \approx 15 \text{ Mpc} , \tag{10.90}$$

using $z_{\rm dec} = 1090$. This corresponds to multipole moment

$$\ell_D \sim k_D d_A^c(z_{\rm dec}) \approx 900 , \tag{10.91}$$

where we have put in $d_A^c(z_{\rm dec}) = 13.8$ Gpc (see section 10.10.2).

This calculation is rather approximate, because of the rapid growth of the photon mean free path (and the typical time between collisions) during recombination, and a more accurate calculation involves an integral over time to take into account this effect. However, the order of magnitude $\ell_D \sim 1000$ is correct, as we see from figure 18, which shows the result of a numerical calculation with and without diffusion damping.

Of the cosmological parameters, the damping depends most strongly on ω_b, since increasing baryon density decreases the photon mean free path before decoupling. Thus for larger ω_b the damping moves to shorter scalesf, i.e. ℓ_D grows. The time evolution of λ_γ before decoupling, and the diffusion scale, is different for different ω_b.

For small ω_b, the time between collisions t_c has already become quite large through the dilution of the baryon density by the expansion of the universe, and the growth of λ_γ relies less on the fast reduction of free electron density during recombination.

10.9 The complete C_ℓ spectrum

As we have discussed, the CMB anisotropy has three contributions (see (10.65)), the effective temperature effect,

$$\frac{1}{4}\delta_\gamma(t_{\rm dec}, \boldsymbol{x}_{\rm ls}) + \Phi(t_{\rm dec}, \boldsymbol{x}_{\rm ls}) \ , \tag{10.92}$$

the Doppler effect,

$$-\boldsymbol{v}\cdot\hat{\boldsymbol{n}}(t_{\rm dec}, \boldsymbol{x}_{\rm ls}) \ , \tag{10.93}$$

and the integrated Sachs–Wolfe effect,

$$2\int_{\rm dec}^{o}\dot{\Phi}{\rm d}t \ . \tag{10.94}$$

Because C_ℓ is quadratic in the perturbations, it includes cross-terms between these three effects.

The calculation of the full C_ℓ proceeds much as the calculation of just the ordinary Sachs–Wolfe part (which (which dominates the temperature anisotropy on super-Hubble scales) in section 10.6.1, but now with the full $\delta T/T$. Since all perturbations are proportional to the primordial curvature perturbation, the C_ℓ spectrum is proportional to $\mathcal{P}_\mathcal{R}(k)$ (with integrals over the spherical Bessel functions $j_\ell(kx)$, like in (10.58), to get from k to ℓ).

The difference is that instead of the constant proportionality factor $(\delta T/T)_{SW} = -\frac{1}{5}\mathcal{R}$, we have a k-dependent proportionality resulting from the evolution (including e.g. the acoustic oscillations) of the perturbations.

In figure 19 we show the full C_ℓ spectrum and the different contributions to it. Because the Doppler effect and the effective temperature effect are almost completely off-phase, their cross term gives a negligible contribution.

Since the ISW effect is relatively weak, it contributes more via its cross terms with the Doppler effect and effective temperature than directly. The cosmological model used for figure 19 has $\Omega_\Lambda = 0$, so there is no late ISW effect (which would contribute at the very lowest ℓ), and the ISW effect shown is the early ISW effect due to radiation contribution to the expansion law. This effect contributes mainly to the first peak and to the left of it, explaining why the first peak is so much higher than the other peaks. It also shifts the first peak position slightly to the left and changes its shape.

10.10 Cosmological parameters and CMB anisotropy

Let us finally consider the effect of the various cosmological parameters on the C_ℓ spectrum. It is the most important single observational data set for determining (or constraining) cosmological parameters because it has a rich structure, which we can measure with a precision that no other cosmological observation can match, and because it depends on several cosmological parameters. The latter property is

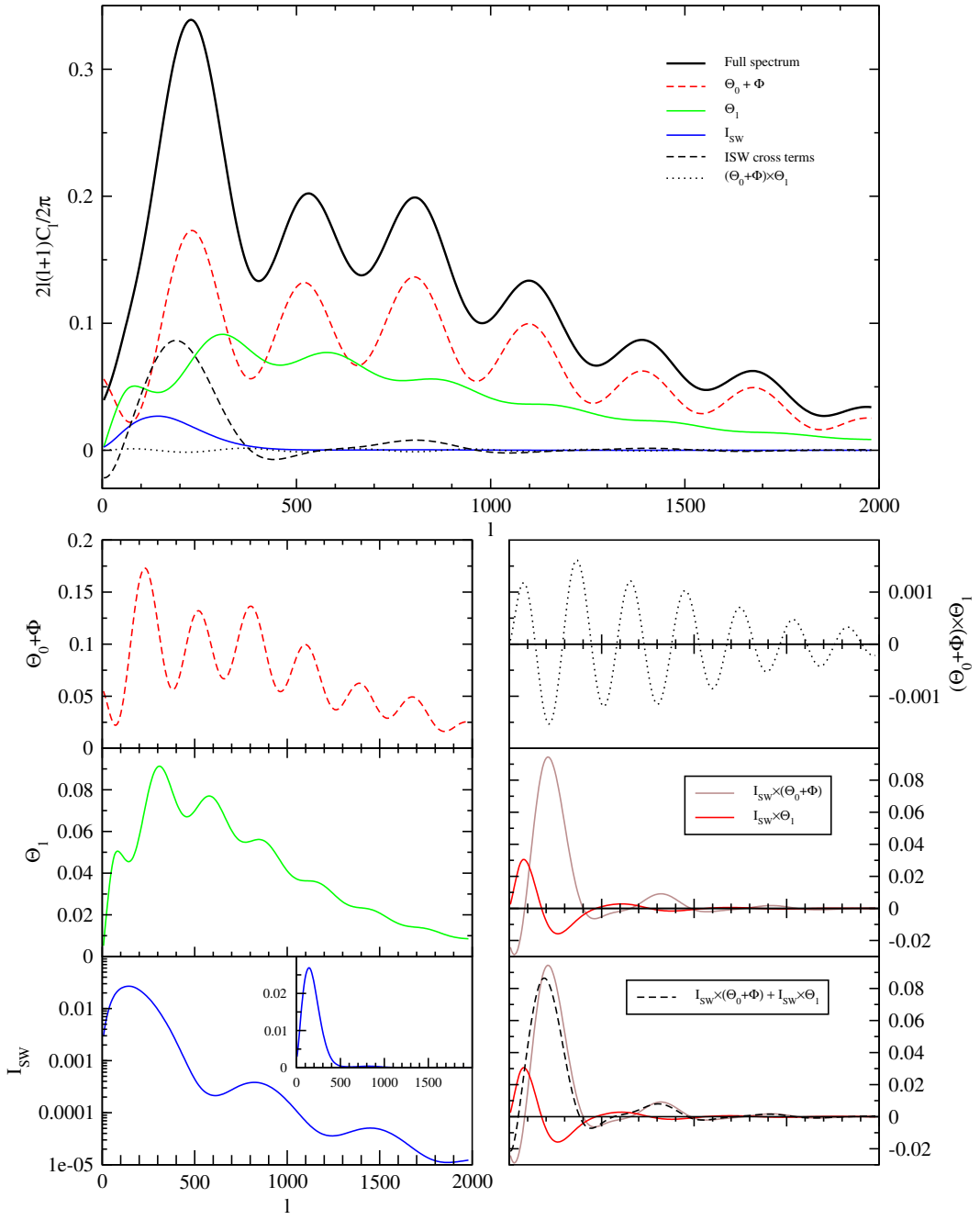


Figure 19: The full C_ℓ spectrum calculated for the cosmological model $\Omega_0 = 1$, $\Omega_\Lambda = 0$, $\omega_m = 0.2$, $\omega_b = 0.03$, $A = 1$, $n = 1$, and the different contributions to it. Here Θ_1 denotes the Doppler effect. Figure and calculation by R. Keskitalo.

both a strength and a weakness: the CMB anisotropy has only a couple of main features (overall amplitude and the positions and heights of the peaks and troughs), so it used to be that you couldn't determine more than a handful of independent parameters from the data. This is because different parameters affect the same features in similar ways, so that we only get a constraint on their combination. Such parameters are called *degenerate*. However, precise observations, in particular by Planck, have been break degeneracies via subtle features of the CMB, such as polarisation and gravitational lensing, which we will not have time to discuss.

The CMB anisotropy pattern is set by the physics at decoupling, and it is then modified as the CMB passes through the universe to be observed today. The CMB pattern at decoupling is determined by the primordial spectrum and the densities of photons, neutrinos, baryons, and cold dark matter. The photon density is precisely known from the CMB mean temperature, and (assuming zero neutrino chemical potential) this also fixes the density of neutrinos. In the case of many inflationary models, the primordial spectrum is a power-law, characterised by the amplitude and the spectral index. In summary, the physics at decoupling is determined by

- $\omega_b = \Omega_{b0}h^2$ the physical baryon density
- $\omega_m = \Omega_{m0}h^2$ the physical matter density
- A amplitude of primordial scalar perturbations (at pivot scale k_*)
- n_s spectral index of primordial scalar perturbations

The angular scale at which the pattern is seen changes as the universe evolves, and this is the main effect of the physics after decoupling on the CMB anisotropy. In addition, the CMB photons scatter off free charges after reionisation. In principle, this effect is determined in terms of the physical parameters at decoupling, but the physics involved in stellar formation and other relevant processes is too complicated to calculate from first principles. Therefore the effect of reionisation is encoded in the parameter τ called the *optical depth* (discussed in section 10.10.6). Roughly speaking, τ gives the probability that a given photon scatters at least once between decoupling and today. We could therefore take the model-independent CMB post-decoupling CMB parameters as

- $d_A^c(z_{\rm dec})$ comoving angular diameter distance to the last scattering surface
- τ optical depth

The angular diameter distance is a general model-independent quantity. In a given FLRW model, it is determined by the spatial curvature and the expansion history, as we have discussed. In the ΛCDM model, where there is vacuum energy and spatial curvature, the angular diameter distance can be replaced by these two parameters, so we have

- Ω_0 total density parameter
- $\Omega_{\Lambda 0}$ vacuum energy density parameter
- τ optical depth .

In addition to changing the angular diameter distance, vacuum energy and spatial curvature also contribute to the CMB anisotropy via the ISW effect, as discussed earlier. The decoupling and post-decoupling parameters add up to a total of seven parameters. Since spatial curvature is not needed to explain the observations and inflation predicts that it is negligible, in the ΛCDM model it is put to zero, $\Omega_0 = 1$. The term ΛCDM model, or the *standard cosmological model*, or the *concordance model* refers to the model parametrised by the six parameters above. We will keep spatial curvature in the discussion to show what effect it would have.

Other choices are also used. With the CosmoSlider[8] you check what effect changing the cosmological parameters has when the set of independent parameters is $\{\omega_b, \omega_{\rm cdm}, h, A, n_s, \tau\}$, where $\omega_{\rm cdm} \equiv \omega_m - \omega_b$.

There are many addtional possible cosmological parameters that could affect the C_ℓ spectrum, for example

- m_{ν_i} neutrino masses
- w constant dark energy equation of state
- w_0, w_a dark energy equation of state and its derivative today (see (3.88))
- r, n_t relative amplitude and spectral index of
- α_s running of the spectral index tensor perturbations
- B, $n_{\rm iso}$ amplitude and spectral index of primordial isocurvature perturbations,
- $A_{\rm cor}$, $n_{\rm cor}$ and their correlation with the primordial curvature perturbations

In particular, r raises C_ℓ at the low multipoles. We assume here that these additional parameters have no impact, i.e. they have the standard values

$$m_{\nu_i} = 0 \ , \ r = \alpha_s = B = A_{\rm cor} = 0 \ , \quad w = w_0 = -1 \ , w_a = 1 \tag{10.95}$$

to the accuracy that matters for C_ℓ observations.[9] There is no sign in the present-day CMB data for non-zero values of these parameters. On the other hand, significant deviations from zero can be consistent with the data, and may be discovered by future other observations; we discussed some hints for non-zero w_a and corresponding deviation of w_0 from -1 in section 3.2.9. The primordial isocurvature perturbation parameters quantify the possibility that the primordial scalar perturbations are not adiabatic, and therefore are not completely determined by the comoving curvature perturbation $\mathcal{R}$.

The assumption that these additional parameters have no impact leads to a determination of the standard parameters with a precision that may be too optimistic, since the standard parameters can have degeneracies with the additional parameters.

[8] https://aarhuscosmology.github.io/CosmoSliderWeb/

[9] Nowadays in CMB analysis the standard minimal assumption is to take the sum of the neutrino masses to be 0.06 eV, since this is minimum compatible with the mass differences measured in neutrino oscillation experiments.

10.10.1 Independent vs. dependent parameters

The above is our choice of the set of independent cosmological parameters. Then Ω_{m0}, Ω_{b0} and H_0 (or h) are then dependent (or derived) parameters, since they are determined by

$$\Omega_0 = \Omega_{m0} + \Omega_{\Lambda 0} \quad \Rightarrow \quad \Omega_{m0} = \Omega_0 - \Omega_{\Lambda 0} \tag{10.96}$$

$$h = \sqrt{\frac{\omega_m}{\Omega_{m0}}} = \sqrt{\frac{\omega_m}{\Omega_0 - \Omega_{\Lambda 0}}} \tag{10.97}$$

$$\Omega_{b0} = \frac{\omega_b}{h^2} = \frac{\omega_b}{\omega_m}(\Omega_0 - \Omega_{\Lambda 0}) \ . \tag{10.98}$$

In particular, the Hubble constant H_0 is a derived parameter. The CMB temperature anisotropy has no sensitivity to H_0 except via the angular diameter distance to the last scattering surface.

Different choices of independent parameters are possible within our 7-dimensional parameter space (e.g. we could have chosen H_0 to be an independent parameter and let $\Omega_{\Lambda 0}$ to be a dependent parameter instead). They can be though of as different coordinate systems in this seven-dimensional space. *It is not meaningful to discuss the effect of one parameter without specifying the set of independent parameters!*

Some choices of independent parameters are better than others, the above choice is one possibility. There are other choices are more geared to minimising parameter degeneracy. For example, the Planck analysis uses the sound horizon angle θ_s instead of $\Omega_{\Lambda 0}$ as an independent parameter, since it is directly determined by the acoustic peak separation, and thus less subject to degeneracies. However, the determination of the dependent parameters from it is in turn more complicated. The independent parameters have been chosen so that they correspond as directly as possible to physics affecting the C_ℓ spectrum and thus to observable features in it. We want the effects of our independent parameters on the observables to be as uncorrelated as possible to avoid parameter degeneracy.

In particular,

- ω_m (not Ω_{m0}) determines $z_{\rm eq}$ and $k_{\rm eq}$, and thus e.g. the magnitude of the early ISW effect and which scales enter during matter- or radiation-dominated epoch.
- ω_b (not Ω_{b0}) determines the baryon/photon ratio and thus e.g. the relative heights of the odd and even peaks.
- $\Omega_{\Lambda 0}$ (not $\Omega_{\Lambda 0}h^2$) determines the late ISW effect.

There are many effects on the C_ℓ spectrum, and parameters act on them in different combinations.

In the following plots made with CAMB we see the effect of these parameters on C_ℓ by varying one parameter at a time around a *reference model*, whose parameters have the following values.

Independent parameters:

$$\begin{aligned} \Omega_0 &= 1 & \qquad \Omega_{\Lambda 0} &= 0.7 \\ A &= 1 & \qquad \omega_m &= 0.147 \\ n &= 1 & \qquad \omega_b &= 0.022 \\ \tau &= 0.1 \end{aligned}$$

which give the dependent parameters

$$\begin{aligned} \Omega_{m0} &= 0.3 & h &= 0.7 \\ \Omega_{c0} &= 0.2551 & \omega_c &= 0.125 \\ \Omega_{b0} &= 0.0449 \end{aligned}$$

The meaning of setting $A = 1$ is just that the resulting C_ℓ still need to be multiplied by the true value of A^2. (In this model the true value should be about $A = 5 \times 10^{-5}$ to agree with observations.) If we really had $A = 1$, perturbation theory of course would not be valid! This is a relatively common practice, since the effect of changing A is so trivial, it doesn't make sense to plot C_ℓ separately for different values of A.

10.10.2 Sound horizon angle

The positions of the acoustic peaks of the C_ℓ spectrum provides us with a measurement of the sound horizon angle

$$\theta_s \equiv \frac{r_s^c(t_{\rm dec})}{d_A^c(t_{\rm dec})}$$

We can use this in the determination of the values of the cosmological parameters, once we have calculated how this angle depends on those parameters. It is the ratio of two quantities, the sound horizon at photon decoupling, $r_s^c(t_{\rm dec})$, and the angular diameter distance to the last scattering, $d_A^c(t_{\rm dec})$.

Angular diameter distance to last scattering

The angular diameter distance $d_A^c(t_{\rm dec})$ to the last scattering surface we have already calculated and it is given by (10.26) as

$$d_A^c(t_{\rm dec}) = H_0^{-1} \frac{1}{\sqrt{1-\Omega_0}} \sinh\left(\sqrt{1-\Omega_0} \int_{\frac{1}{1+z_{\rm dec}}}^{1} \frac{{\rm d}a}{\sqrt{\Omega_0(a-a^2) - \Omega_{\Lambda 0}(a-a^4) + a^2}} \right) \quad (10.99)$$

from which we see that it depends on the three cosmological parameters H_0, Ω_0 and $\Omega_{\Lambda 0}$. Here $\Omega_0 = \Omega_{m0} + \Omega_{\Lambda 0}$, so we could also say that it depends on H_0, Ω_{m0}, and $\Omega_{\Lambda 0}$, but it is easier to discuss the effects of these different parameters if we keep Ω_0 as an independent parameter, instead of Ω_{m0}, since the "geometry effect" of the curvature of space, which determines the relation between the comoving angular diameter distance d_A^c and the comoving distance d^c, is determined by Ω_0.

1. The comoving angular diameter distance is inversely proportional to H_0 (directly proportional to the Hubble distance H_0^{-1}).

2. Increasing Ω_0 decreases $d_A^c(t_{\rm dec})$ in relation to $d_P^c(t_{\rm dec})$ because of the geometry effect.

3. With a fixed $\Omega_{\Lambda 0}$, increasing Ω_0 decreases $d_A^c(t_{\rm dec})$, since it means increasing Ω_{m0}, which has a decelerating effect on the expansion. With a fixed present expansion rate H_0, deceleration means that expansion was faster earlier $\Rightarrow$ universe is younger $\Rightarrow$ there is less time for photons to travel as the universe cools from $T_{\rm dec}$ to T_0 $\Rightarrow$ last scattering surface is closer to us.

4. Increasing $\Omega_{\Lambda 0}$ (with a fixed Ω_0) increases $d_A^c(t_{\rm dec})$, since it means a larger part of the energy density is in dark energy, which has an accelerating effect on the expansion. With fixed H_0, this means that expansion was slower in the past $\Rightarrow$ universe is older $\Rightarrow$ more time for photons $\Rightarrow$ last scattering surface is further out $\Rightarrow$ $\Omega_{\Lambda 0}$ increases $d_A^c(t_{\rm dec})$.

Here 2 and 3 work in the same direction: increasing Ω_0 decreases $d_A^c(t_{\rm dec})$, but the geometry effect (2) is stronger. See figure 14 for the case $\Omega_{\Lambda 0} = 0$, where the dashed line (the comoving distance) shows effect (3) and the solid line (the comoving angular diameter distance) the combined effect (2) and (3).

However, now we have to take into account that, in our chosen parametrisation, H_0 is not an independent parameter, but

$$H_0^{-1} \propto \sqrt{\frac{\Omega_0 - \Omega_{\Lambda 0}}{\omega_m}} \ ,$$

so that via H_0^{-1}, Ω_0 increases and $\Omega_{\Lambda 0}$ decreases $d_A^c(t_{\rm dec})$, which are the opposite effects to those discussed above. For $\Omega_{\Lambda 0}$ this opposite effect wins. See figures 22 and 23.

Sound horizon

To calculate the comoving sound horizon,

$$r_s^c(t_{\rm dec}) = a_0 \int_0^{t_{\rm dec}} \frac{c_s(t)}{a(t)} {\rm d}t = \int_0^{t_{\rm dec}} \frac{{\rm d}t}{a} c_s(t) = \int_0^{a_{\rm dec}} \frac{{\rm d}a}{a \cdot ({\rm d}a/{\rm d}t)} c_s(a) \ , \quad (10.100)$$

we need the speed of sound from (10.68),

$$c_s^2(a) = \frac{1}{3} \frac{1}{1 + \frac{3}{4}\frac{\bar\rho_b}{\bar\rho_\gamma}} = \frac{1}{3} \frac{1}{1 + \frac{3}{4}\frac{\omega_b}{\omega_\gamma} a} \ , \quad (10.101)$$

where the upper limit of the integral is $a_{\rm dec} = 1/(1 + z_{\rm dec})$.

The other element in the integrand of (10.100) is the expansion law $a(t)$ before decoupling. We have

$$a \frac{{\rm d}a}{{\rm d}t} = H_0 \sqrt{\Omega_{\Lambda 0} a^4 + (1 - \Omega_0) a^2 + \Omega_{m0} a + \Omega_{r0}} \ . \quad (10.102)$$

In the integral (10.99) we dropped the Ω_{r0} term, since it is important only at early times, and the integral from $a_{\rm dec}$ to 1 is dominated by late times. Integral (10.100), on the other hand, includes only early times, and now we can instead drop the $\Omega_{\Lambda 0}$ and $1 - \Omega_0$ terms (i.e. we can ignore the effect of curvature and dark energy in the early universe, before photon decoupling), so

$$a \frac{{\rm d}a}{{\rm d}t} \approx H_0 \sqrt{\Omega_{m0} a + \Omega_{r0}} = H_{100} \sqrt{\omega_m a + \omega_r} = \frac{\sqrt{\omega_m a + \omega_r}}{2998 \ {\rm Mpc}} \ , \quad (10.103)$$

where we have written

$$H_0 \equiv h \cdot 100 \frac{\rm km/s}{\rm Mpc} \equiv h \cdot H_{100} = \frac{h}{2997.92 \ {\rm Mpc}} \ . \quad (10.104)$$

Thus the sound horizon is

$$r_s^c(a) = 2998\ \text{Mpc} \int_0^a \frac{c_s(a)\mathrm{d}a}{\sqrt{\omega_m a + \omega_r}} = 2998\ \text{Mpc} \cdot \frac{1}{\sqrt{3\omega_r}} \int_0^a \frac{\mathrm{d}a}{\sqrt{\left(1+\frac{\omega_m}{\omega_r}a\right)\left(1+\frac{3}{4}\frac{\omega_b}{\omega_\gamma}a\right)}} \ . \tag{10.105}$$

Here

$$\omega_\gamma = 2.4702 \times 10^{-5} \qquad \text{and} \tag{10.106}$$

$$\omega_r = \left[1 + \frac{7}{8}N_\nu\left(\frac{4}{11}\right)^{4/3}\right]\omega_\gamma = 1.6904\ , \omega_\gamma = 4.1756 \times 10^{-5} \tag{10.107}$$

are accurately known from the CMB temperature $T_0 = 2.725$ K (and therefore we do not consider them as cosmological parameters in the sense of something to be determined from the C_ℓ spectrum).

Thus the sound horizon depends on the two cosmological parameters ω_m and ω_b,

$$r_s^c(t_{\rm dec}) = r_s^c(\omega_m, \omega_b)$$

From (10.105) we see that increasing either ω_m or ω_b *makes the sound horizon at decoupling,* $r_s^c(a_{\rm dec})$*, shorter*:

- ω_b slows the sound down
- ω_m speeds up the expansion at a given temperature, so the universe cools to $T_{\rm dec}$ in less time.

The integral (10.105) can be done and it gives

$$r_s^c(t_{\rm dec}) = \frac{2998\ \text{Mpc}}{\sqrt{1+z_{\rm dec}}} \frac{2}{\sqrt{3\omega_m R_*}} \ln \frac{\sqrt{1+R_*} + \sqrt{R_* + r_* R_*}}{1+\sqrt{r_* R_*}} \ , \tag{10.108}$$

where

$$r_* \equiv \frac{\bar\rho_r(t_{\rm dec})}{\bar\rho_m(t_{\rm dec})} = \frac{\omega_r}{\omega_m}\frac{1}{a_{\rm dec}} = 0.0459\frac{1}{\omega_m}\frac{1+z_{\rm dec}}{1100} \tag{10.109}$$

$$R_* \equiv \frac{3\bar\rho_b(t_{\rm dec})}{4\bar\rho_\gamma(t_{\rm dec})} = \frac{3\omega_b}{4\omega_\gamma}a_{\rm dec} = 27.6\ , \omega_b\frac{1100}{1+z_{\rm dec}} \ . \tag{10.110}$$

For our reference values $\omega_m = 0.147$, $\omega_b = 0.022$, and $1 + z_{\rm dec} = 1100$[10] we get $r_* = 0.312$ and $R_* = 0.607$ and $r_s^c(t_{\rm dec}) = 143$ Mpc for the sound horizon at decoupling.

Summary

The angular diameter distance $d_A^c(t_{\rm dec})$ is most naturally discussed in terms of H_0, Ω_0, and $\Omega_{\Lambda 0}$, but since these are not the most convenient choice of independent

[10] Photon decoupling temperature, and thus $1 + z_{\rm dec}$, depends somewhat on ω_b, but since this dependence is not easy to calculate (recombination and photon decoupling were discussed in chapter 5), we have mostly ignored this dependence and used the fixed value $1 + z_{\rm dec} = 1100$.

parameters for other purposes, we shall trade H_0 for ω_m according to (10.97). Thus we see that the sound horizon angle depends on 4 parameters,

$$\theta_s \equiv \frac{r_s^c(\omega_m, \omega_b)}{d_A^c(\Omega_0, \Omega_{\Lambda 0}, \omega_m)} = \theta_s(\Omega_0, \Omega_{\Lambda 0}, \omega_m, \omega_b) \ . \tag{10.111}$$

If we keep ω_m and ω_b fixed, we have $r_s^c(t_{\rm dec}) = 143$ Mpc. From the observed value $100\theta_s = 1.04092$ [2] we then have $d_A^c = 13.7$ Gpc $\approx 3H_0^{-1}$, taking $h = 0.7$. For the Einstein-de Sitter model we have $d_A^c(1090) \approx 1.97 H_0^{-1} \approx 8.4$ Gpc, so the observed distance to the last scattering surface is about 50% larger than predicted by the FLRW model without dark energy or spatial curvature.

We get a rough estimate of the angular diameter distance from the observed angular size of the extrema on the CMB sky as follows.

$$\begin{aligned} d_A^c(z_{\rm dec}) &= \frac{r_s^c(t_{\rm dec})}{\theta_s} \approx \frac{\frac{1}{\sqrt{3}} d_{\rm hor}(t_{\rm dec})}{\theta_s}(1 + z_{\rm dec}) \\ &\approx \frac{180^\circ}{\pi \theta_s(^\circ)} \sqrt{3} t_{\rm dec}(1 + z_{\rm dec}) \approx 21 \text{ Gpc} \ , \end{aligned} \tag{10.112}$$

where we have approximated $r_s = d_{\rm hor}/\sqrt{3}$ and $d_{\rm hor} = 3t$, and $\theta_s(^\circ)$ is θ_s in degrees. This value is within a factor of 2 of the real result. However, the difference between the observation and the Einstein-de Sitter result for d_A^c is only 50%, so this rough approximation cannot be used to rule out the Einstein-de Sitter model, we have to use a more precise value for the sound horizon.

10.10.3 Acoustic peak heights

There are a number of effects that change the heights of the acoustic peaks:

1. **The early ISW effect.** The early ISW effect raises the first peak. It is caused by the evolution of Φ because of the effect of the radiation contribution on the expansion law after $t_{\rm dec}$. This depends on the radiation-matter ratio at that time; decreasing ω_m makes the early ISW effect stronger.

2. **Shift of oscillation equilibrium by baryons.** (Baryon drag.) This makes the odd peaks (which correspond to compression of the baryon-photon fluid in the potential wells, decompression on potential hills) higher, and the even peaks (decompression at potential wells, compression on top of potential hills) lower.

3. **Baryon damping.** The time evolution of $R \equiv 3\bar{\rho}_b/4\bar{\rho}_\gamma$ causes the amplitude of the acoustic oscillations to be damped in time roughly as $(1+R)^{-1/4}$. This reduces the amplitudes of all peaks.

4. **Radiation driving.**[11] This is an effect related to horizon scale physics that we have not tried to properly calculate. For scales k which enter during the radiation-dominated epoch, or near matter-radiation equality, the potential Φ decays around the time when the scale enters. The potential keeps changing as

[11] This is also called gravitational driving, which is perhaps more appropriate, since the effect is due to the change in the gravitational potential.

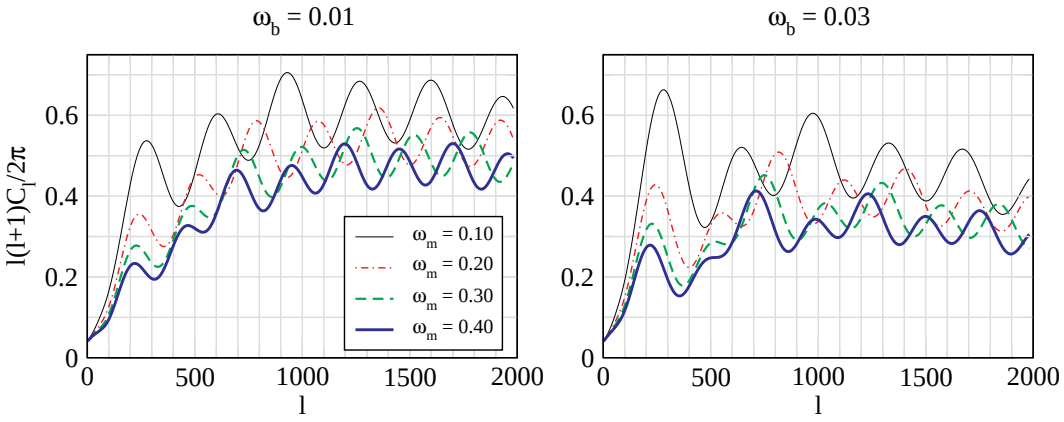


Figure 20: The effect of ω_m. The angular power spectrum C_ℓ is here calculated without the effect of diffusion damping, so that the other effects on peak heights could be seen more clearly. Notice how reducing ω_m raises all peaks, but the effect on the first few peaks is stronger in relative terms, as the radiation driving effect is extended towards larger scales (smaller ℓ). The first peak is raised mainly because the ISW effect becomes stronger. Figure and calculation by R. Keskitalo.

long as the radiation contribution is important, but the largest change in Φ is around horizon entry. Because the sound horizon and Hubble length are comparable, Hubble entry and the corresponding potential decay always happen during the first oscillation period. This means that the baryon-photon fluid is falling into a deep potential well, and therefore is compressed by gravity by a large factor, before the resulting overpressure is able to push it out. Meanwhile the potential has decayed, so it is less able to resist the decompression phase, and the overpressure is able to kick the fluid further out of the well. This increases the amplitude of the acoustic oscillations. The effect is stronger for the smaller scales which enter when the universe is more radiation-dominated, and therefore raises the peaks with a larger peak number n more. Reducing ω_m makes the universe more radiation-dominated, making this effect stronger and extending it towards the peaks with lower peak number n.

5. **Diffusion damping.** Diffusion damping lowers the heights of the peaks. It acts in the opposite direction than the radiation driving effect, lowering the peaks with a larger peak number m more. Because the diffusion damping effect is exponential in ℓ, it wins for large ℓ.

Effects 1 and 4 depend on ω_m, effects 2, 3, and 5 on ω_b. See figures 20 and 21 for the effects of ω_m and ω_b on peak heights.

10.10.4 Effect of Ω_0 and $\Omega_{\Lambda 0}$

These two parameters have only two effects:

1. they affect the sound horizon angle and thus the positions of the acoustic peaks; and

2. they affect the late ISW effect.

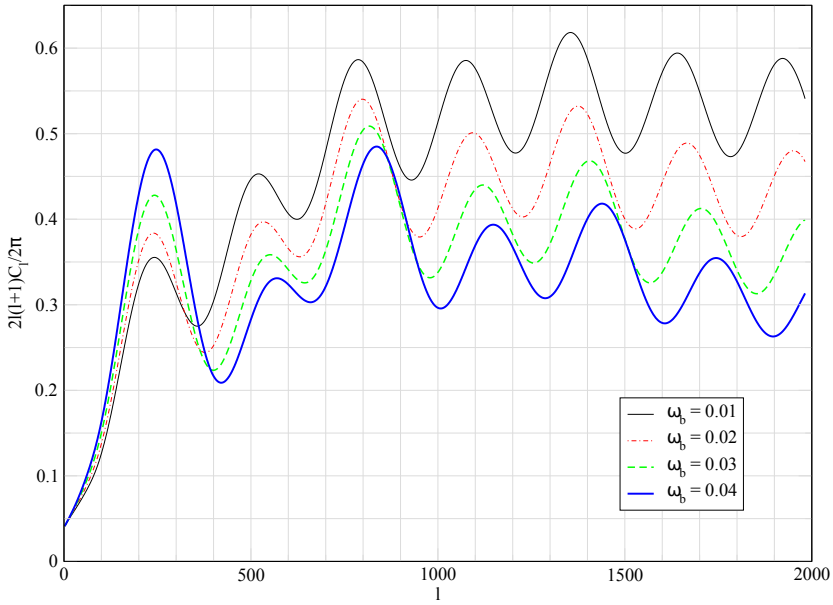


Figure 21: The effect of ω_b. The angular power spectrum C_ℓ is here calculated without the effect of diffusion damping, so that the other effects on peak heights could be seen more clearly. Notice how increasing ω_b raises odd peaks relative to the even peaks. Because of baryon damping there is a general trend downwards with increasing ω_b. This figure is for $\omega_m = 0.20$. Figure and calculation by R. Keskitalo.

See figures 22 and 23. Since the late ISW effect is in the region of the C_ℓ spectrum where the cosmic variance is large, it is difficult to detect. Thus we can in practice only use θ_s to determine Ω_0 and $\Omega_{\Lambda 0}$. Since ω_b and ω_m can be determined quite accurately from C_ℓ acoustic peak heights, the peak separation, (i.e. θ_s), can then be used for the determination of Ω_0 and $\Omega_{\Lambda 0}$. Since we cannot determine two numbers from one, the parameters Ω_0 and $\Omega_{\Lambda 0}$ are degenerate. CMB temperature anisotropy observations alone cannot be used to determine them both. Other cosmological observations (like the power spectrum $P_\delta(k)$ from large scale structure, or the SNIa redshift-distance relationship) are needed to break this degeneracy.

A fixed θ_s together with fixed ω_b and ω_m determine a line on the (Ω_0, $\Omega_{\Lambda 0}$) -plane. See figure 24. Derived parameters such as h vary along that line. As you can see from figures 22 and 23, changing Ω_0 (around the reference model) affects θ_s more strongly than changing $\Omega_{\Lambda 0}$. (This is because the ratio of the vacuum energy density to the matter density grows like a^3, while the ratio of the spatial curvature to the matter density grows only like a.) This means that the orientation of the line is such that $\Omega_{\Lambda 0}$ varies more rapidly along that line than Ω_0. Therefore using additional constraints from other cosmological observations, e.g. the determination of h from the distance ladder, which select a short section from that line, gives us a fairly good determination of Ω_0, leaving the allowed range for $\Omega_{\Lambda 0}$ still quite large. As discussed already in chapter 1, the distance ladder determination of h is currently in strong contradiction with the result from the CMB, and this contradiction is not resolved by spatial curvature.

Therefore it is often said that CMB measurements have determined that $\Omega_0 \sim 1$, i.e. that the universe is spatially flat. However, this is misleading. First, the

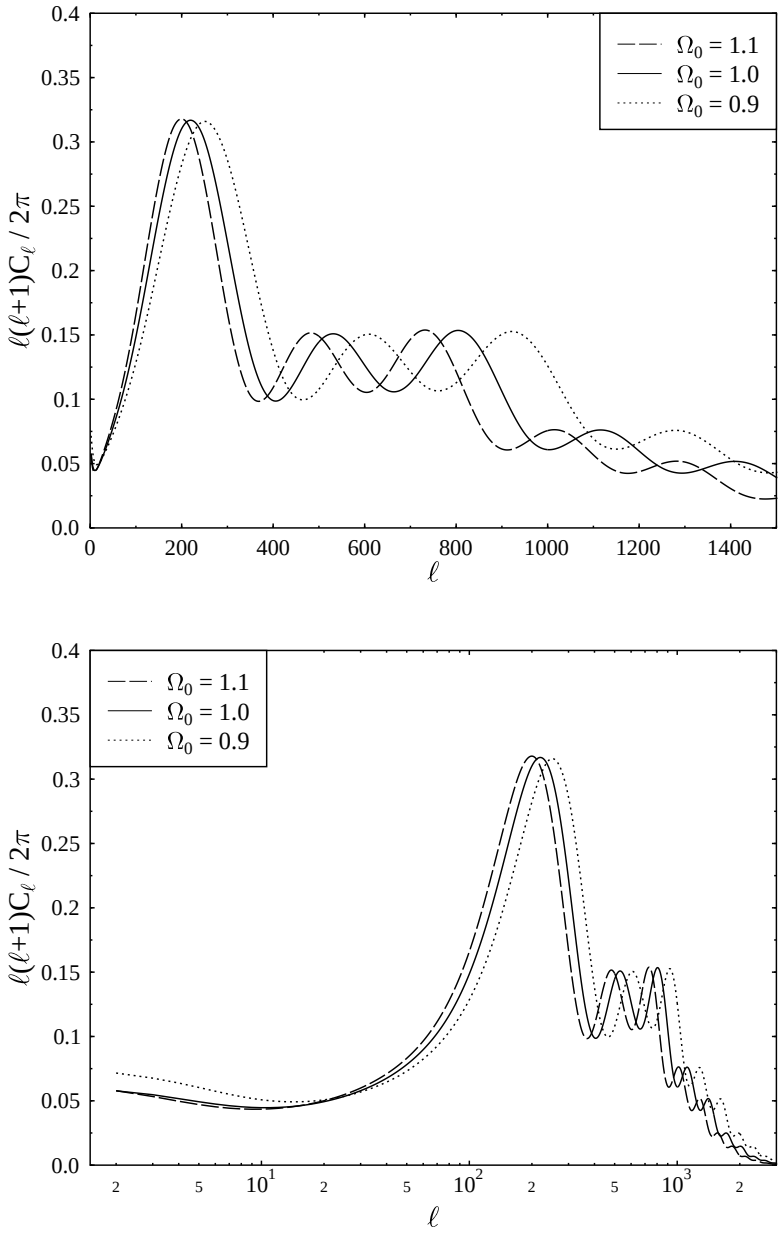


Figure 22: The effect of changing Ω_0 from its reference value $\Omega_0 = 1$. The top panel shows the C_ℓ spectrum with a linear ℓ scale so that details at larger ℓ where cosmic variance effects are smaller can be better seen. The bottom plot has a logarithmic ℓ scale so that the integrated Sachs-Wolfe effect at small ℓ can be better seen. The logarithmic scale also makes it clear that the effect of the change in the sound horizon angle is to stretch the spectrum by a constant factor in ℓ space.

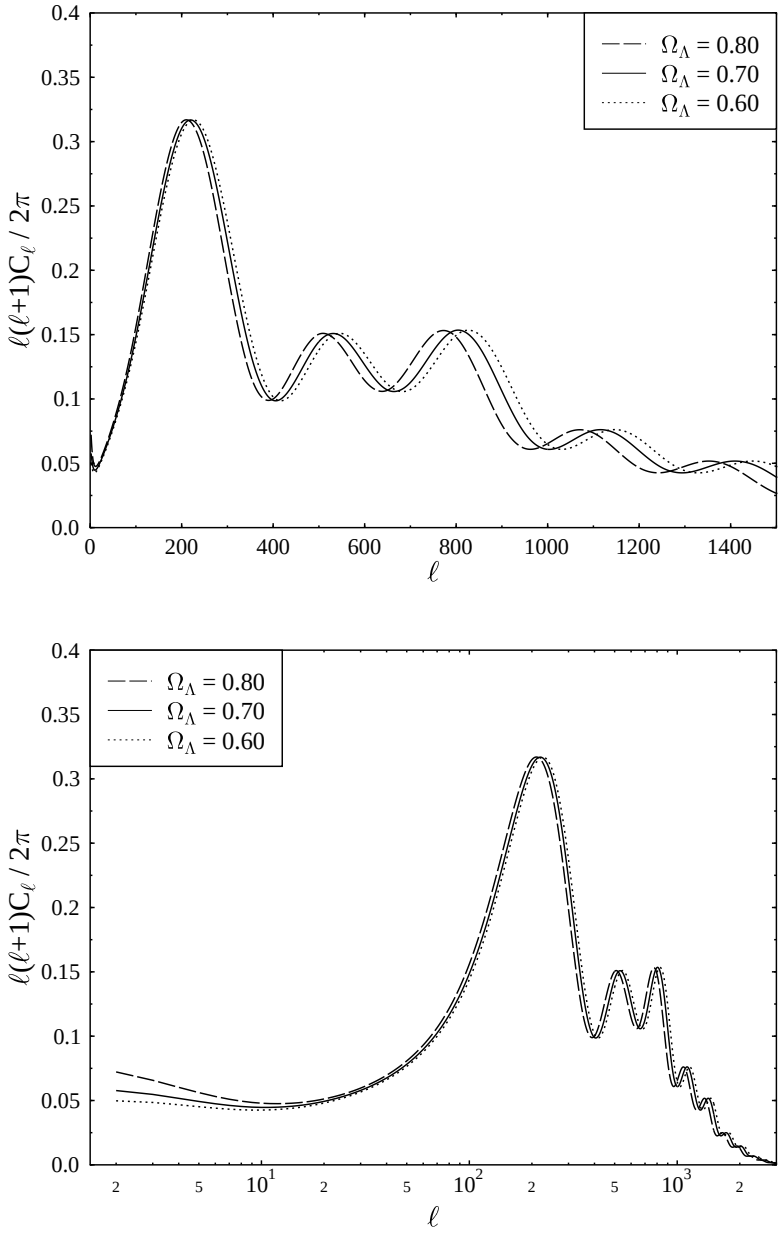


Figure 23: The effect of changing $\Omega_{\Lambda 0}$ from the reference value $\Omega_{\Lambda 0} = 0.7$.

CMB only determines the angular diameter distance to the last scattering surface. Determining the spatial curvature from this requires knowing the expansion history $H(z)$, in other words the constraints on the spatial curvature are model-dependent. The correct statement is that assuming that the universe is described by the ΛCDM model plus spatial curvature, the CMB data shows that the universe is close to spatially flat.

10.10.5 Effect of the primordial spectrum

The effect of changing the primordial spectrum is simple. Raising the amplitude A raises the C_ℓ also, and changing the primordial spectral index tilts C_ℓ. See figures 25 and 26.

10.10.6 Effect of the optical depth due to reionisation

After radiation from the first stars reionises the free atoms and molecules, CMB photons may scatter from the resulting free electrons. The optical depth τ due to reionisation is the expectation number of such scatterings per CMB photon. Its value is $\tau = 0.0544 \pm 0.0042$ [2], i.e. most CMB photons do not scatter at all. The rescattering causes additional polarisation of the CMB, and CMB polarisation measurements are the best way to determine τ.

Because of this scattering, not all CMB photons come from the location on the last scattering surface they seem to come from. The effect of the rescattered photons is to mix up signals from different directions and therefore reduce the CMB anisotropy. The reduction factor on $\delta T/T$ is $e^{-\tau}$ and on the C_ℓ spectrum $e^{-2\tau}$. However, this does not affect the largest scales, scales larger than the area from which the rescattered photons reaching us from a certain direction originally came from. Such a large-scale anisotropy has affected all such photons the same way, and thus is not lost in the mixing. See figure 27.

10.10.7 Effect of ω_b and ω_m

These parameters affect both the position (through θ_s) and the heights of the acoustic peaks. The latter effect is the more important, since the two parameters have a distinct impact on the peak heights, allowing an accurate determination of these parameters, whereas their effect on θ_s is degenerate with Ω_0 and $\Omega_{\Lambda 0}$.

Especially ω_b has a characteristic effect on peak heights. Increasing ω_b raises the odd peaks and reduces the even peaks, because it shifts the balance of the acoustic oscillations (the $-R\Phi$ effect). This shows the most clearly in the first and second peaks.[12] Raising ω_b also shortens the damping scale k_D^{-1} due to photon diffusion, increasing the corresponding damping scale ℓ_D. This has the effect of raising C_ℓ at large ℓ. See figure 28.

Increasing ω_m makes the universe more matter-dominated at $t_{\rm dec}$ and therefore reduces the early ISW effect, making the first peak lower. This also affects the shape of the first peak.

[12] There is also an overall "baryon damping effect" on the acoustic oscillations which we have not calculated. It is due to the time dependence of $R \equiv 3\bar{\rho}_b/4\bar{\rho}_m$, which reduces the amplitude of the oscillation by about $(1+R)^{-1/4}$. This explains why the third peak in figure 28 is no higher for $\omega_b = 0.030$ than it is for $\omega_b = 0.022$.

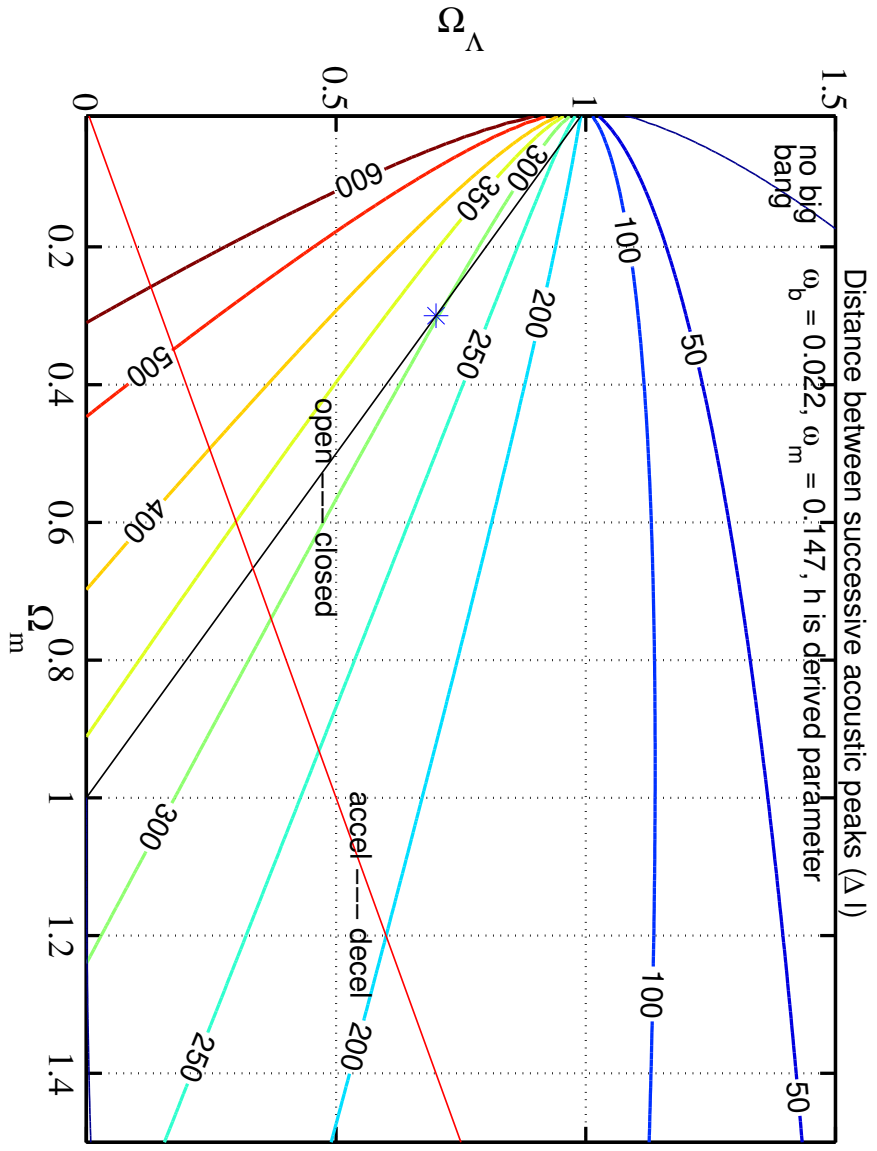


Figure 24: The lines of constant sound horizon angle θ_s on the $(\Omega_{m0},\Omega_{\Lambda 0})$ plane for fixed ω_b and ω_m. The numbers on the lines refer to the corresponding acoustic scale $\ell_A \equiv \pi/\theta_s$ ($\sim$ peak separation) in multipole space. Figure by J. Väliviita.

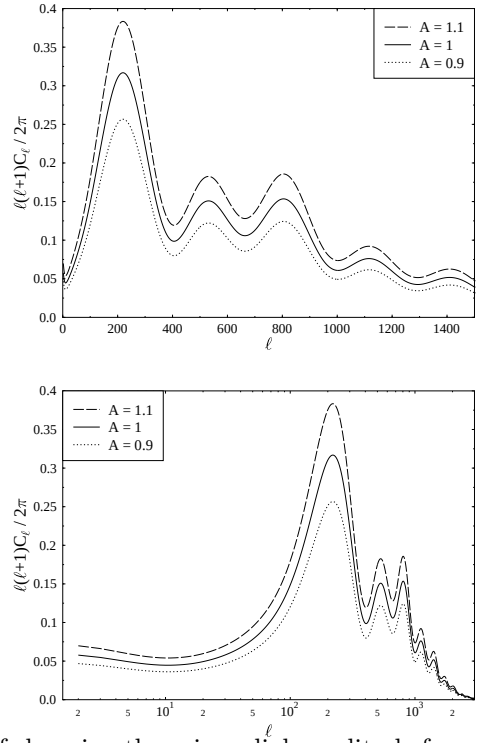


Figure 25: The effect of changing the primordial amplitude from the reference value $A = 1$.

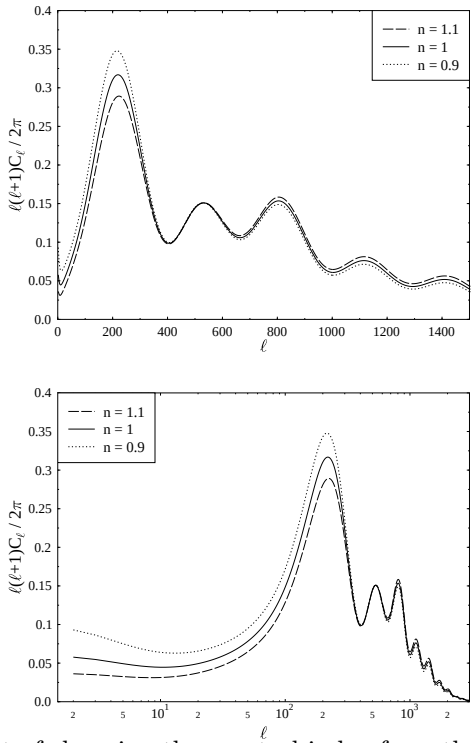


Figure 26: The effect of changing the spectral index from the reference value $n = 1$.

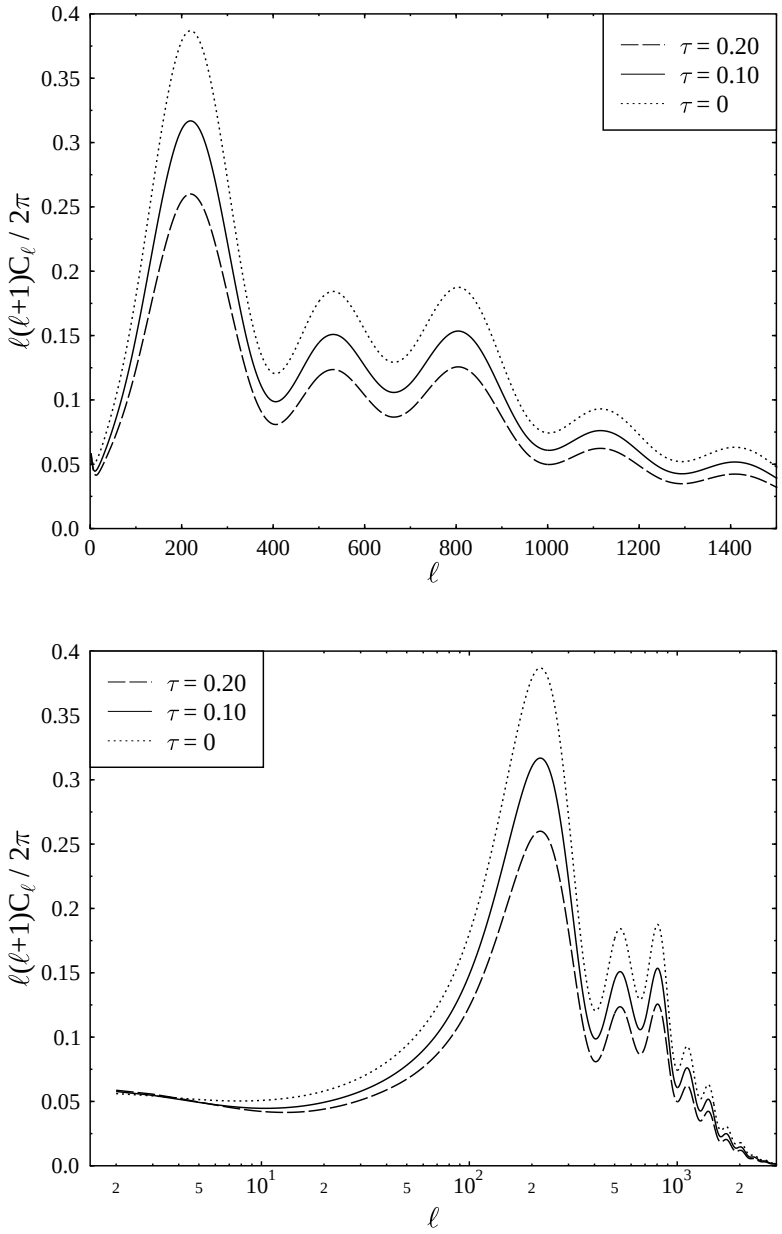


Figure 27: The effect of changing the optical depth from the reference value $\tau = 0.1$.

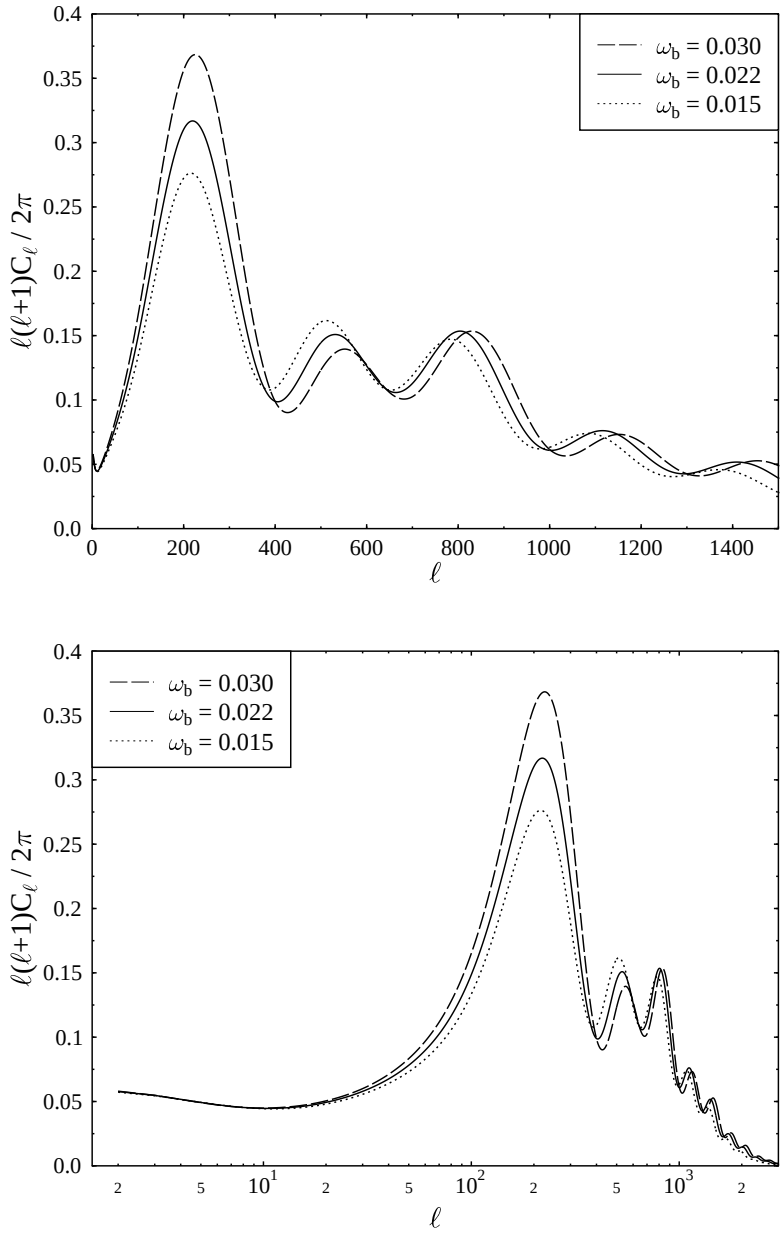


Figure 28: The effect of changing the physical baryon density parameter from the reference value $\omega_b = 0.022$.

The "radiation driving" effect is most clear in the second to fourth peaks. Reducing ω_m raises these peaks by making the universe more radiation-dominated at the time the scales corresponding to these peaks enter, and thus strengthening this radiation driving. The fifth and further peaks correspond to scales that have anyway essentially the full effect, whereas for the first peak this effect is anyway weak. (We see instead the ISW effect in the first peak.) See figure 29.

10.11 Values of the cosmological parameters

The most important single cosmological data set for determining the values of the cosmological parameters is the Planck satellite measurement of the CMB anisotropy. It used to be the case that because of degeneracies of cosmological parameters in the CMB data (for example, the CMB is sensitive to the vacuum energy and spatial curvature mostly via the angular diameter distance) CMB observations had to be supplemented by other cosmological data for a good determination of the main cosmological parameters. However, with current precise data that measures different aspects of the CMB (temperature, polarisation, lensing, ...), it is possible to determine parameters pretty well just from CMB data, but it is still often combined with other data to get more precise results.

The most prominent feature in large-scale structure surveys is the turnover scale in the 3-dimensional matter power spectrum $P_\delta(k)$. It mainly measures the combination $\Omega_{m0}h$, since this determines where $P_\delta(k)$ turns down. The turn is at $k_{\rm eq}$ which is proportional to $\omega_m \equiv \Omega_{m0}h^2$, but since in these surveys the distances to the galaxies are deduced from their redshifts (therefore these surveys are also called galaxy redshift surveys), which give the distances only up to the Hubble constant H_0, these surveys determine $h^{-1}k_{\rm eq}$ instead of $k_{\rm eq}$. This cancels one power of h. Having $\Omega_{m0}h^2$ from CMB and $\Omega_{m0}h$ from the galaxy surveys, gives us both h and $\Omega_{m0} = \Omega_0 - \Omega_{\Lambda 0}$, which breaks the Ω_0-$\Omega_{\Lambda 0}$ degeneracy.

These measurements of $P_\delta(k)$ are now so accurate that the small residual effect from the *baryon acoustic oscillations* (BAO) before photon decoupling can be seen as a weak wavy pattern. This is the same structure seen in the C_ℓ but much fainter, since now the baryons have fallen into the CDM potential wells, and the CDM was only mildly affected by these oscillations in the baryon-photon fluid. The half-wavelength of this pattern corresponds to the same sound horizon distance $r_s^c(t_{\rm dec})$ in both cases.[13] The redshift at which the pattern is seen is however much smaller, so this gives a measurement of $d_A^c(z)$ at a different redshift[14]. Another way to break the Ω_0-$\Omega_{\Lambda 0}$ degeneracy is to use the redshift-distance relationship from SNIa observations.

However, the more datasets one puts together, the more assumptions are involved in the analysis, so constraints from large combinations of data should be treated more cautiously. In Table I we give the values of standard parameters as determined either from Planck data alone or Planck supplemented by BAO data [2]. It is assumed that $\Omega_0 = 1$. The first column gives the mean value and the error bars. The first column includes only CMB data, including on the temperature anisotropy,

[13] To be accurate, the best $t_{\rm dec}$ value to represent the effect in $P_\delta(k)$ is not exactly the same as for C_ℓ, since photon decoupling was not instantaneous, and in the galaxies we see the effect on matter and in the CMB the effect on photons.

[14] In fact, the BAO signal gives a combination of $d_A(z)$ and $H(z)$.

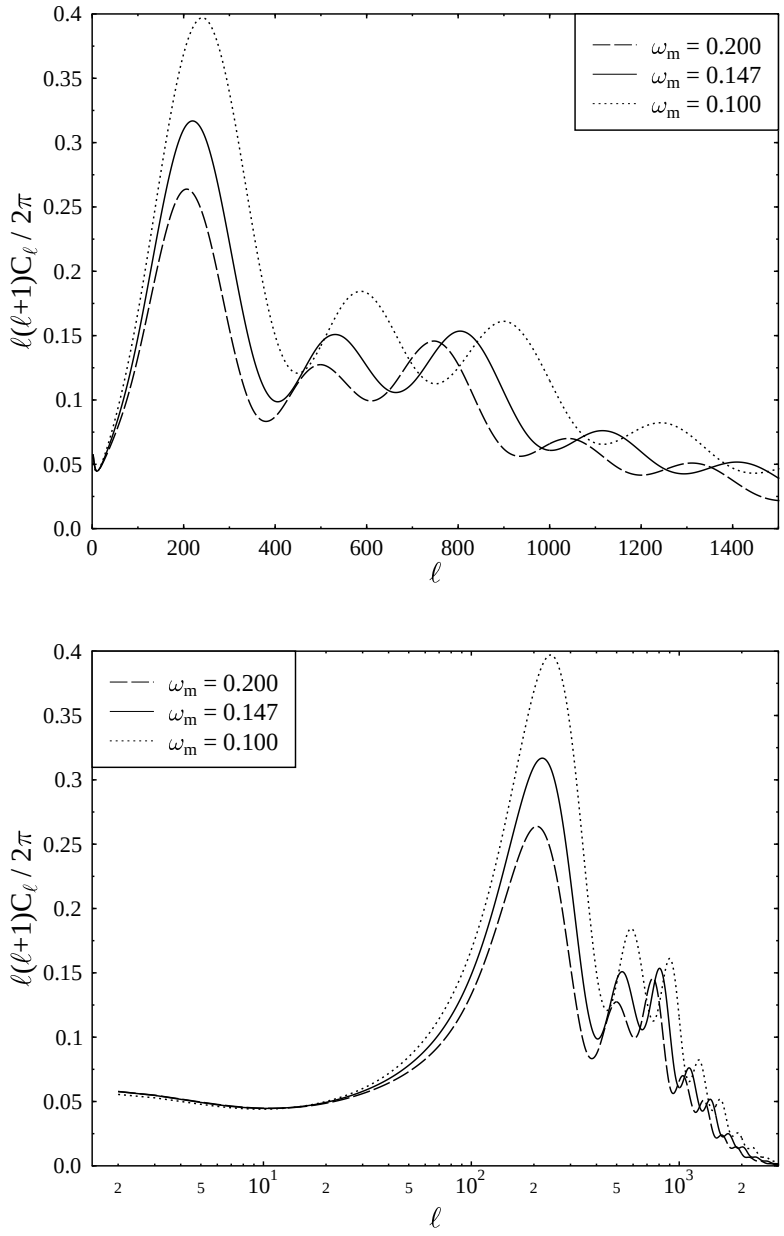


Figure 29: The effect of changing the physical matter density parameter from the reference value $\omega_m = 0.147$.

Table I: Standard parameters

	Planck TT,TE,EE+lowE+lensing	Planck TT,TE,EE+lowE+lensing+BAO
$100\omega_b$	2.237 ± 0.015	2.242 ± 0.014
ω_c	0.1200 ± 0.0012	0.11993 ± 0.00091
$100\theta_s$	1.04092 ± 0.00031	1.04101 ± 0.00029
τ	0.0544 ± 0.0073	0.0561 ± 0.0071
n_s	0.9649 ± 0.0042	0.9665 ± 0.0038

Table II: Derived parameters

	Planck TT,TE,EE+lowE+lensing	Planck TT,TE,EE+lowE+lensing+BAO
Ω_{m0}	0.3153 ± 0.0073	0.3111 ± 0.0056
$100h$	67.36 ± 0.54	67.66 ± 0.42

polarisation, and lensing. The second column also includes BAO. In Table II we list some related derived parameters, and in Table III we give limits on some non-standard parameters. In table III the error bars are 95% confidence limits.

The BBN result $100\omega_b = 2.205 \pm 0.043$ has not been used here, but we see that the determination of the baryon density from the CMB is consistent with the BBN value. The agreement between these two independent datasets (abundances of light elements and anisotropies on the microwave sky), one of which probes the physics between about one second and one hour, and the other at around 380 000 years is remarkable. It increases our confidence that the basic physical picture of the evolution of the universe is correct. Indeed, BBN and CMB are two of the most important pieces of observational support for the standard cosmological model.

The parameters in Table III are derived under the assumption that the non-standard parameters other than the one being considered remain zero. The CMB alone does not give good constraints on the dark energy equation of state, as it mostly affects $d_A^c(z_{\rm dec})$, and is thus degenerate with $\Omega_{\Lambda 0}$. The upper limits given for the sum of neutrino masses $\sum m_\nu$ and the ratio r of tensor perturbations to scalar perturbations are 95% confidence limits. (Here r is quoted at the pivot scale 0.002 Mpc^{-1}.) We see that there is no indication in the data for a deviation of these additional parameters from their standard values. Including data from the BICEP2/Keck telescope brings the limit down to $r < 0.036$ at the pivot scale 0.05 Mpc^{-1} [6], as shown in figure 30.

In conclusion, all cosmological data are almost consistent with a *vanilla universe*, i.e. a spatially flat ΛCDM model with adiabatic and Gaussian primordial density perturbations, described by the six cosmological parameters $\Omega_{\Lambda 0}$, ω_m, ω_b, A, n, τ. (Although τ is not a fundamental parameter: it is just a simple parametrisation of the physics of reionisation, which in principle could be derived from astrophysical evolution but in practice this is too difficult.) The "almost" is important here: as discussed in chapter 1 and in section 3.2.9, the Hubble tension and hints for a time-

Table III: Additional parameters

	Planck TT, TE, EE+lowE+lensing	Planck TT, TE, EE+lowE+lensing+BAO
$\sum m_\nu$	< 0.241 eV	< 0.12 eV
w	$-1.57^{+0.50}_{-0.40}$	-1.04 ± 0.10
Ω_{K0}	$-0.011^{+0.013}_{-0.012}$	0.0007 ± 0.0037
$\frac{\mathrm{d}n}{\mathrm{d}\ln k}$	-0.005 ± 0.013	-0.004 ± 0.013
r	< 0.101	< 0.106

varying dark energy of state are are challenging the vanilla universe, but there is still no theoretical resolution of the Hubble tension and no confirmation of the time evolution of the equation of state, and the situation is under intense investigation.

References

[1] Planck collaboration, N. Aghanim et al., *Planck 2013 results. XXVII. Doppler boosting of the CMB: Eppur si muove*, *Astron. Astrophys.* **571** (2014) A27, [1303.5087].

[2] Planck collaboration, N. Aghanim et al., *Planck 2018 results. VI. Cosmological parameters*, *Astron. Astrophys.* **641** (2020) A6, [1807.06209].

[3] M. Vonlanthen, S. Räsänen and R. Durrer, *Model-independent cosmological constraints from the CMB*, *JCAP* **08** (2010) 023, [1003.0810].

[4] D. H. Lyth and A. R. Liddle, *The primordial density perturbation: Cosmology, inflation and the origin of structure*. 2009.

[5] R. Durrer, *The Cosmic Microwave Background*. Cambridge University Press, Cambridge, 2008, 10.1017/CBO9780511817205.

[6] BICEP, Keck collaboration, P. A. R. Ade et al., *Improved Constraints on Primordial Gravitational Waves using Planck, WMAP, and BICEP/Keck Observations through the 2018 Observing Season*, *Phys. Rev. Lett.* **127** (2021) 151301, [2110.00483].

[7] A. G. Riess et al., *A Comprehensive Measurement of the Local Value of the Hubble Constant with 1 km s^{-1} Mpc^{-1} Uncertainty from the Hubble Space Telescope and the SH0ES Team*, *Astrophys. J. Lett.* **934** (2022) L7, [2112.04510].

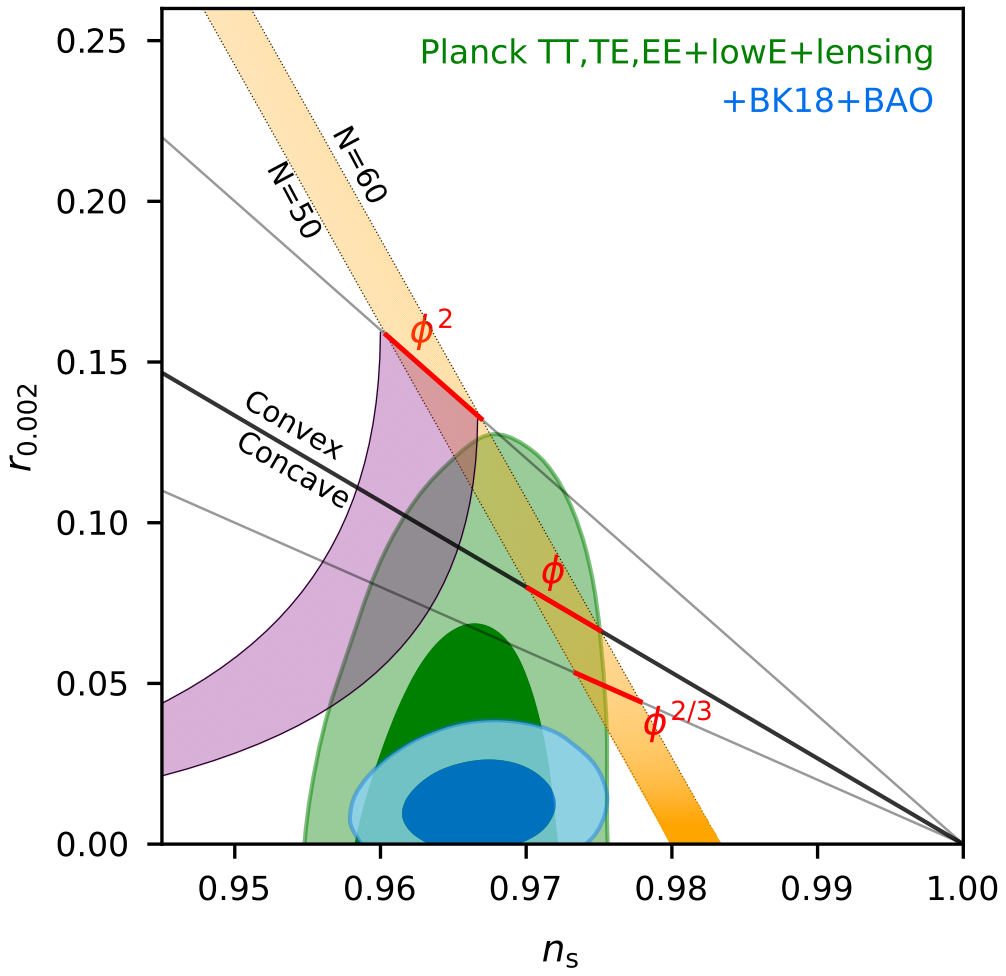


Figure 30: Constraints on the scalar perturbation spectral index n_s and the tensor-to-scalar ratio r from the Planck satellite data alone (wide contours) and combined with BICEP2/Keck and BAO data (narrow contours) [6]. Straight lines show the predictions of power-law potentials, with the number of e-folds corresponding to the pivot scale k_* varying along the line.